International Journal of Nanomedicine

Dovepress
Taylor & Francis Group

Open Access Full Text Article

ORIGINAL RESEARCH

Preparation and Antitumor Activity of METTL3 SiRNA Nanoparticles Carried by Hypoxia Sensitive Polymer (mPEG-Azo-PEI)

Zhenglu Yin[1], Zhaoxiang Meng[1], Bo Chen[1], Junya Wang[1], Aihua Zhang[1], Yan Shen[2], Xiaojia Tang[1], Shunyan Lin[3]

[1]Department of Rehabilitation, Northern Jiangsu People's Hospital, Northern Jiangsu People's Hospital Affiliated to Yangzhou University, Yangzhou City, Jiangsu, 225001, People's Republic of China; [2]Department of Pharmaceutics, China Pharmaceutical University, Nanjing, Jiangsu, 211100, People's Republic of China; [3]Department of Anesthesiology, Northern Jiangsu People's Hospital, Northern Jiangsu People's Hospital Affiliated to Yangzhou University, Yangzhou City, Jiangsu, 225001, People's Republic of China

Correspondence: Shunyan Lin, Department of Anesthesiology, Northern Jiangsu People's Hospital, Northern Jiangsu People's Hospital Affiliated to Yangzhou University, Yangzhou City, Jiangsu, 225001, People's Republic of China, Email 3922744619@qq.com

Purpose: The clinical application of small interfering RNA (siRNA) therapy is limited by instability, inefficient tumor targeting, and inadequate responsiveness to the hypoxic tumor microenvironment. Therefore, this study aimed to construct a hypoxia-sensitive polymer-based nanocarrier to improve siRNA delivery efficiency and enhance antitumor effects in colorectal cancer (CRC).

Methods: A hypoxia-sensitive polymer (mPEG-Azo-PEI) was synthesized and its cytotoxicity was assessed using the 3-(4,5-dimethylthiazol-2-yl)-2,5-diphenyltetrazolium bromide (MTT) assay. The polymer was loaded with siRNA targeting the METTL3 gene to form nanoparticles, which were then optimized and characterized. Coumarin-loaded nanoparticles were also prepared to study the cellular uptake in HCT116 cells under hypoxic conditions. The Antitumor effects were evaluated via MTT and real-time polymerase chain reaction (RT-PCR) in vitro and in vivo, and a rectal cancer model was established using HCT116 cells in nude mice. Tumor size, weight, and histology (HE staining) were assessed, and RT-PCR analyzed METTL3 ex-pression.

Results: The CMC of mPEG-Azo-PEI was 0.001687 mg/mL, indicating good self-assembly stability under dilution conditions. The optimized mPEG-Azo-PEI@siRNA2 nanoparticles exhibited a mean particle size of 141.34 ± 2.31 nm, a PDI of 0.213 ± 0.011, and a zeta potential of +21.76 ± 1.76 mV. Hypoxia-triggered release reached ~95% within 24 h, compared with ~10% under normoxic conditions. Coumarin uptake by HCT116 cells was enhanced under hypoxic conditions, indicating improved intracellular delivery. In vitro, the nanoparticles inhibited tumor cell proliferation, with IC50 values of 1.133 (normoxia) and 0.481 (hypoxia) nM. In vivo, mPEG-Azo-PEI@siRNA2 significantly suppressed tumor growth and improved body weight. RT-PCR confirmed the downregulation of METTL3, aligning with tumor suppression.

Conclusion: These results demonstrated that hypoxia-sensitive mPEG-Azo-PEI@siRNA2 nanoparticles effectively delivered siRNA2 and inhibited HCT116 cell proliferation, offering a promising hypoxia-activated targeting strategy for colon cancer therapy.

Keywords: siRNA nanoparticles, mPEG-Azo-PEI, hypoxia, antitumor, drug delivery

Introduction

The most abundant apparent transcriptomic modification in eukaryotic MRNAs is 6-methyladenine (N6-methyladenosine, m6A), which accounts for approximately 0.1% to 0.4% of all adenosines and occurs through methylation at N6 adenine in RNA.[1,2] Although it was discovered in the 1970s, it was not until the development of enzymology and high-throughput detection technology in recent years that m6A kinetics were truly connected with various diseases, development, and cell processes in eukaryotes.[3,4] Currently, scientists have identified more than 10000 m6A peaks in human transcripts (25%). These peaks are mostly located on the common motif with RRACH characteristics (R=G or A, H=A, C or U), wherein they are located in region of long exon, near the termination codon and 3 'untranslated region.[5,6] Methylation of m6A RNA has been implicated in various studies owing to its significant and

https://doi.org/10.2147/IJN.S588018
Received: 30 December 2025
Accepted: 1 April 2026
Published: 14 April 2026

multifaceted role in tumor formation and development.[7] As a dynamic and reversible process of modification,[8] the methylation of m6A RNA proceeds from catalytic formation to functional realization, which is principally regulated by m6A methyltransferase complexes (encoders), m6A demethylases (erasers), and m6A reading proteins (readers). The m6A methyltransferase complex can catalyze the modification of m6A in RNA with S-adenosyl-methionine as the methyl donor.[2,9] The main components are Wilms tumor-1-associated protein (WTAP) and methyl-transferase-like protein-3 and-14 (METTL3 and METTL14).[10,11] As a methyl-transferase was first discovered and the core subunit of the complex, METTL3 plays a vital role in catalysis. Therefore, the m6A modification activity was almost completely lost when METTL3 was knocked out.

Hypoxia is a common phenomenon in solid tumor tissues, and hypoxia in tumor cells may be regarded as one of the initiating factors of malignant tumor progression. Hypoxia makes cancer cells more aggressive during epithelial-mesenchymal transition (EMT), which plays a vital role in tumor invasion and metastasis process. During this process, primary cancer cells transform from static epithelial cells to mesenchymal cells, amid their ability to migrate, and demonstrate strong invasion potential. Recent studies have suggested a close relationship between EMT and the tumor microenvironment. Hypoxia is one of the most important microenvironment characteristics of colorectal cancer (CRC).[12,13]

In CRC, accumulating evidence indicates that methyltransferase-like 3 (METTL3), the core catalytic component of the m6A methyltransferase complex, functions as an oncogenic driver. Elevated METTL3 expression has been associated with enhanced tumor proliferation, invasion, and poor prognosis in CRC patients.[14] Mechanistically, METTL3 promotes CRC progression by regulating m6A modification of key oncogenic transcripts and activating tumor-promoting signaling pathways, such as the JAK1/STAT3 axis.[15] Moreover, recent studies have reported that METTL3 contributes to chemotherapy resistance and immune evasion in CRC by modulating tumor microenvironment–related signaling axes.[16,17] In addition, CRC progression is frequently accompanied by therapeutic resistance, and tumor hypoxia is a well-recognized contributor to aggressive phenotypes and treatment failure.[18]

A growing body of evidence indicates a link between the survival rate of post-surgery patients and abnormal expression of METTL3.[19,20] Thus, METTL3 as an effective tumor prognostic marker, may play a key role in tumor initiation and progression.[21] Despite the therapeutic potential of siRNA, its clinical translation remains significantly limited by several delivery-related challenges.[22] RNA interference (RNAi)-based therapy, particularly small interfering RNA (siRNA), enables sequence-specific silencing of disease-driving genes at the post-transcriptional level.[23] Compared with conventional small-molecule chemotherapy, siRNA offers high target specificity, the ability to modulate previously "undruggable" genes, and reduced off-target cytotoxicity when appropriately delivered. In addition, chemo–gene combinatorial regimens often require co-delivery of agents with distinct physicochemical properties, which complicates formulation, dose matching, and spatiotemporal release control. In the context of CRC, siRNA-mediated suppression of oncogenic drivers such as METTL3 provides a rational strategy to interfere with tumor proliferation, invasion, and therapeutic resistance at the molecular level. However, efficient and safe delivery remains the principal barrier to clinical translation. Naked siRNA is highly susceptible to rapid degradation by serum nucleases and exhibits poor systemic stability in circulation.[24] In addition, due to its negative charge and relatively large molecular weight, siRNA demonstrates limited cellular uptake and inefficient membrane permeability.[25] Even after internalization, siRNA is frequently trapped within endosomes, resulting in insufficient cytoplasmic release and reduced gene silencing efficiency.[26] Furthermore, in solid tumors such as CRC, the abnormal tumor microenvironment, including hypoxia, high interstitial pressure, and poor vascularization, further restricts effective drug penetration and distribution.[27] Therefore, overcoming these biological barriers represents a critical challenge in the development of effective siRNA-based therapeutics. In this regard, we sought to construct a hypoxic environment-sensitive polymer, which can be used to wrap siRNA that targets the METTL3 gene, and thus prepare nanoparticles for tumor-targeted delivery.

Current therapeutic strategies for CRC include surgery, chemotherapy, targeted therapy, and immunotherapy. Combination approaches such as chemo-gene therapy have been investigated to enhance therapeutic efficacy and overcome drug resistance by simultaneously targeting multiple oncogenic pathways.[28] Immunotherapy has also emerged as an important treatment modality, however, its efficacy in CRC remains limited to specific molecular subtypes, such as microsatellite instability-high (MSI-H) tumors.[29] Complementarily, siRNA-based strategies offer a direct means of

silencing oncogenic drivers irrespective of mutational status, and may complement or sensitize tumors to existing therapies. Phototherapy-based strategies, including photodynamic and photothermal therapy, have also been explored for CRC treatment owing to their spatial selectivity and minimal invasiveness.[30] These limitations further highlight the importance of microenvironment-responsive systems capable of functioning in hypoxic tumor regions. In this setting, siRNA-mediated gene silencing provides a rational approach to suppress oncogenic drivers and resistance-associated pathways at the mRNA level, with target specificity determined by sequence design. In addition, siRNA-based interventions may be integrated with established modalities to enhance treatment responses and broaden benefit beyond subsets of patients who respond to current therapies.

Compared with conventional siRNA delivery systems, the present study introduces a hypoxia-responsive mPEG-Azo-PEI nanoparticle system that enables environment-triggered release specifically under tumor hypoxic conditions. By integrating tumor microenvironment responsiveness with METTL3 gene silencing, this strategy aims to enhance therapeutic specificity, improve intracellular release efficiency, and overcome key biological barriers associated with siRNA therapy in colorectal cancer. To our knowledge, this work represents a novel approach that combines hypoxia-targeted polymer design with epigenetic gene regulation for CRC treatment.

Materials and Methods

Materials

Shanghai Macklin Biochemical Technology Co., Ltd. provided azobenzene-4,4-dicarboxylic acid, methoxy polyethylene glycol amine (2000 Da), polyethylene imine (1800 Da), 1-ethyl - (3-dimethyl-aminopropyl) carbo-diimide (EDC), triethylamine (Et3N), pyridine, N, N-dimethyl amide (DMF), 1-hydroxy-benzotriazole (HOBt), pyrene, tetrahydrofuran, trypsin, and TBE buffer. Human Keloid Fibroblast cells (HKF, Catalog number: CP-H235), Human Colon Tumor Cell Line 116 (HCT116, Catalog number: CL-0096), Dulbecco's modified eagle medium (DMEM), and roswell park memorial institute 1640 Medium (RPMI-1640) were supplied by Procell Life Science &Technology Co., Ltd. (China). All the cell lines were authenticated and tested for mycoplasma contamination before use. Lipofectamine 2000 and the TRIzol reagent were purchased from Invitrogen. Chloroform, isopropanol, 75% ethanol, diethyl pyrocarbonate (DEPC) water, acetate buffer, and phosphotungstic acid were purchased from Sinopharm Chemical Reagent Co. Ltd. Reverse Transcription Kits were purchased from Nanjing Vazyme Biotechnology Co. Ltd. SYBR Premium Ex Taq was supplied by Takara. MTT, DMSO, and Phosphate-buffered saline (PBS) were purchased from Beijing Solarbio Technology Co. Ltd. 4',6-diamidino-2-phenylindole (DAPI) staining solution, Triton X-100 and 5-fluorouracil (5-Fu) were purchased from Biyotime Biotechnology Research Institute. β-Nicotinamide adenine dinucleotide, reduced form (NADH; Aladdin Biochemical Technology Co., Ltd., Shanghai, China; Cat. No. N106933) and nitroreductase (NTR; recombinant, expressed in E. coli; Sigma-Aldrich (Merck), St. Louis, MO, USA; Cat. No. N9284; specific activity ≥100 U/mL) were purchased from Aladdin and Sigma-Aldrich, respectively. Anti-METTL3 antibody (Cat. #86132) was purchased from Cell Signaling Technology (CST, USA).

Synthesis of mPEG-Azo-PEI

Azobenzene-4,4 '-dicarboxylic acid (20 μM) was dissolved in pyridine, EDC (20 μM), NHS (20 μM), and a catalytic amount of DMAP was added. The carboxyl group was activated by stirring for 1 h. mPEG-NH2 (MW, 2.0 K) (10 μM) was then dissolved in chloroform and added dropwise to the pyridine solution described above for overnight reaction at room temperature. After the reaction, the solvent was removed by rotary evaporation and the product mPEG-Azo was purified by dialysis using pure water. The mPEG-Azo was purified by dialysis (MWCO 3.5 kDa) against deionized water for 48 h with frequent water changes (more frequent changes in the first 12 h, followed by changes every 8–12 h thereafter). After dialysis, the solution was lyophilized to obtain mPEG-Azo.

After dissolving mPEG-Azo (5.3 μM) into pyridine, EDC (10.6 μM), NHS (10.6 μM), and a catalytic amount of DMAP were added. The carboxyl group was activated by stirring for 1 h. PEI (MW, 1.8 K) (5.3 μM) was dissolved in chloroform, added dropwise to the pyridine solution described above, and the reaction was stirred overnight at room

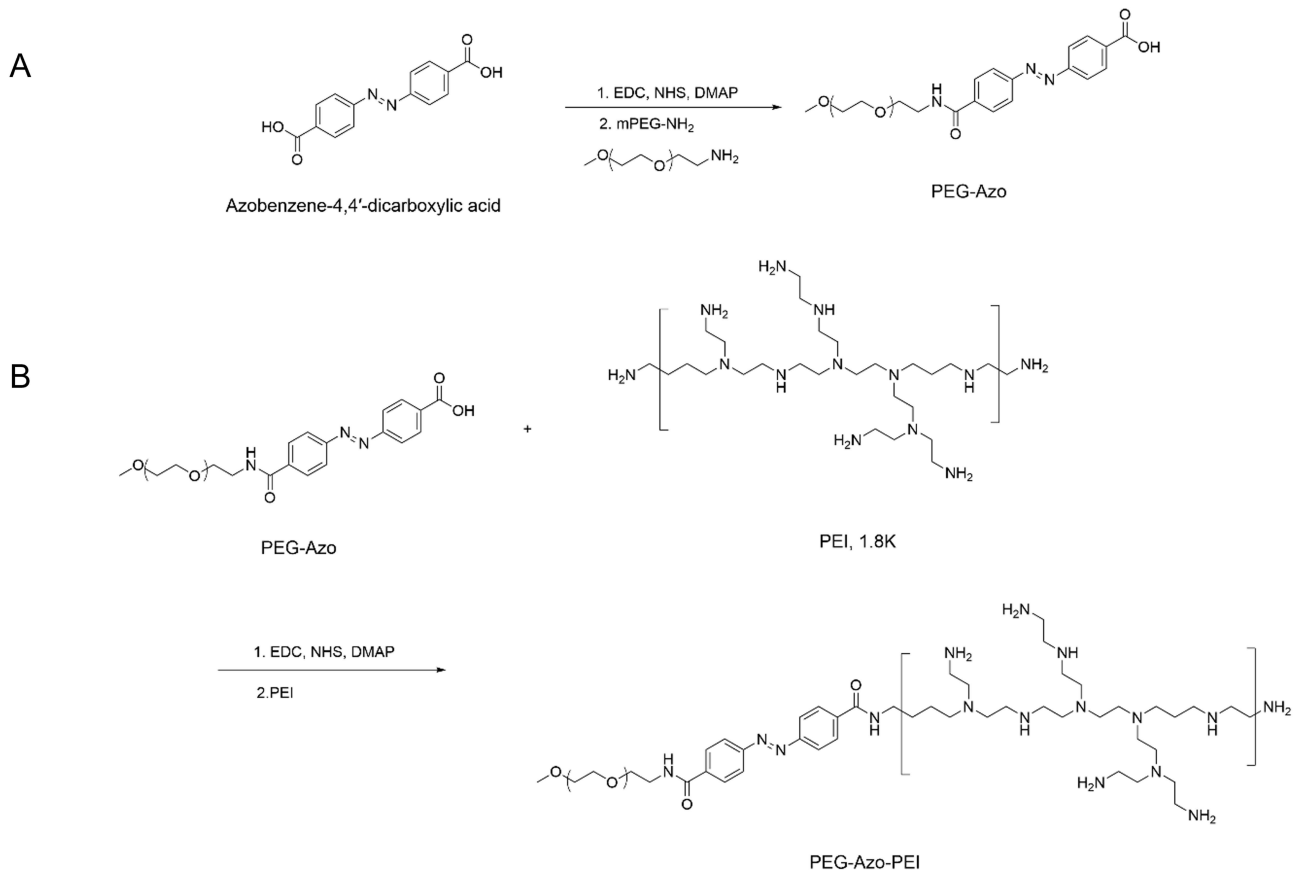

Figure 1 Synthesis of mPEG-Azo-PEI. (**A**) Schematic illustration of the synthetic route of mPEG-Azo-PEI. (**B**) Chemical structure of the final product.

temperature. After the reaction was complete, the solvent was removed by rotary evaporation and the product mPEG-Azo -PEI was purified using the procedure described above (Figure 1).

Determination of Encapsulation Efficiency and Drug Loading

The encapsulation efficiency (EE) and drug loading (DL) of mPEG-Azo-PEI@siRNA2 nanoparticles were determined by measuring the amount of free siRNA in the supernatant after centrifugation. Briefly, the nanoparticle suspension was centrifuged at 15000 rpm for 15 min at 4 °C, and the supernatant containing unloaded siRNA was collected. The concentration of free siRNA was quantified by UV spectrophotometry at 260 nm. The amount of siRNA loaded into the nanoparticles was calculated by subtracting the amount of free siRNA from the total amount of siRNA initially added. EE and DL were calculated according to the following equations:

EE = (Amount of siRNA loaded / Total amount of siRNA added) × 100%

DL = (Amount of siRNA loaded / Total nanoparticle weight) × 100%

Cytotoxicity of mPEG-Azo-PEI

HKF and HCT116 cells at the logarithmic growth stage were inoculated into 96-well culture plates at 5×10^4/well density. Using 5% carbon dioxide incubator, we inoculated the cells at 37 °C for 24 h. After full attachment of the cells to the plate wall, various concentrations of the polymer solution (0.1, 0.2, 0.5, 1, 5, 10, 20, and 50 μg/mL) were added. The control group consisted of untreated cells, and each experiment was performed in triplicate. Cells were cultured for 48 h under both normal and hypoxic conditions. After discarding the culture medium, 200 μL DMEM was added to each well. Subsequently, 40 μL of MTT solution was added and the cells were cultured for 4 h under different conditions. Subsequently, the culture medium was discarded and 200 μL of DMSO was added to each well before shaking on an

oscillator for 10 min (100 rpm). Later, we used the enzyme marker (570 nm) for detection, and the cell morphology was observed and photographed with a random field of view selected by an inverted microscope. The cell survival rate was calculated using the following formula:

Cell survival rate = (absorbance of sample hole − absorbance of normal culture control group)/absorbance of normal culture control group × 100%.

Preparation and Selection of siRNA Loaded Polymer Nanoparticles

siRNA

To counteract the METTL3 sequence (NM_019852.5), three siRNAs were designed and synthesized (with modifications required to increase siRNA stability).

siRNA1:

guide (5'→3') AGCUGCACUUCAGACGAAUUAUCAA

passenger (5'→3') UUGAUAAUUCGUCUGAAGUGCAGCU

siRNA2:

guide (5'→3') CCACCUCAGUGGAUCUGUUGUGAUA

passenger (5'→3') UAUCACAACAGAUCCACUGAGGUGG

siRNA3:

guide (5'→3') ACUGCUUGGUUGGUGUCAAAGGAAA

passenger (5'→3') UUUCCUUUGACACCAACCAAGCAGU

Briefly, Lipofectamine 2000 (Invitrogen, Carlsbad, CA) was used to transfect siRNA, according to the manufacturer's specifications.

Construction of Nanoparticles

siRNAs were dissolved in acetate buffer (10 mM, pH 3.0) to a final concentration of 0.4 mg/mL. PEG-Azo-PEI was dissolved in ethanol at a final concentration of 10 mg/mL.

The ratio of siRNA: PEG-Azo-PEI= 1:5 (w/w), siRNA and PEG-Azo-PEI ethanol solutions were mixed and vortexed for 1 min. The PBS buffer (pH 7.4) was used as the dialysate to obtain the corresponding nanoparticles. For clarity, the siRNA-loaded mPEG-Azo-PEI system is consistently referred to as "nanoparticles" throughout the manuscript.

Expression of METTL3 mRNA in HCT116 by Three siRNA Loaded Polymer Nanoparticle

Logarithmic HCT116 cells were harvested, digested with trypsin, and centrifuged (1000 rpm for 10 min). Afterwards, we discarded the supernatant prior to the addition of a suitable amount of DMEM to complete the medium for resuspension of the cells. After cell counting, the cell concentration was adjusted to 2×10^5 cells/mL. Subsequently, we added the cells into 6-well plates with 2 mL of cells into each well, wherein we set three wells for each group. The culture was maintained in a 5% carbon dioxide incubator at 37 °C until the cells adhered to the wall. The culture medium was discarded and 2 mL of drug-containing serum (5 nM siRNA1, 10 nM siRNA1, 5 nM siRNA2, 10 nM siRNA2, 5 nM siRNA3, 10 nM siRNA3, and blank siRNA) was added. The blank control group was supplemented with 2 mL of medium for each group, and three wells were used for each group. After completing the above procedure, cells were cultured for 48 h in 5% carbon dioxide incubator at 37 °C. In addition, when the grouping and dosage were consistent with the above procedures, we changed the culture conditions to hypoxic culture. Specifically, cells were incubated in a tri-gas incubator under hypoxic conditions (1% O_2, 5% CO_2, and 94% N_2; pO_2 approximately 7 mmHg) at 37 °C for 48 h.

To detect the relative expression of METTL3 mRNA in each group, we used TRIzolTM reagent (Invitrogen, Carlsbad, CA) to extract relevant total RNA from different groups of cells. The specific method was as follows: cells from each group were cultured without digestion. Others were digested and lysed by adding a certain volume of TRIzol reagent at a ratio of 10 cm^2/mL and allowed to stand for 5 min at ambient temperature to make the lysis uniform. Subsequently, 200 μL of chloroform was added to the obtained cracking solution, which was vigorously shaken for 15s, thoroughly mixed, and allowed to settle at the ambient temperature for 3 min. Next, we collected 450 μL of supernatant

after 15 min of centrifugation (4 °C, 12000 rpm) and added to the same volume of isopropyl alcohol solution before we shook and mixed thorough. Subsequently, we allowed it to settle for another 10 min before centrifugation again (12000 rpm, 10 min, 4 °C), discarding the supernatant and reserving the precipitate. After addition of 75% ethanol (1 mL) to the precipitate, we centrifuged (7500 rpm, 5 min, 4 °C) and discarded the supernatant, but retained the bottom precipitate (this process was repeated twice). Later on, we added 30 μL of DEPC to the sediment and dissolved at 55 °C for 10 min before refrigeration at −80 °C for storage.

Establishment of RT-PCR Reaction System

After the total RNA samples were dissolved, complementary DNA (cDNA) was synthesized using a reverse transcription kit and used as a template for PCR amplification. The primer sequences are shown in Table 1.

The reference gene was glyceraldehyde-3-phosphate dehydrogenase (GAPDH). Using SYBR Premix Ex-Taq configuration, we performed RT-PCR assaying with the following reaction conditions: 60s of initial polymerization at 95 °C, 15s of denaturation at 95 °C, 30s of annealing at 60 °C, 1 min of extension of the reaction at 72 °C, and completion of 30 cycles. After the extended step of 72 °C for 10 min, we a 2% agarose gel electrophoresis. PCR product density was analyzed using Band Leader software (version 2.2.3), and data were analyzed at the same time. Of note, triplicate measurements were taken, and calculation and normalization of relative expression were accomplished using the $2^{-\Delta\Delta Ct}$ method.

Cell Viability Assay

HCT116 cells cultured for 48 h under normal and hypoxic conditions were collected before the medium was discarded and 200 μL of DMEM was added to each well. Next, 40 μL of MTT solution was added and incubation continued according to different conditions for 4 h. Subsequently, the medium was discarded, and 200 μL of DMSO was added to each well before oscillating the cells in an oscillator for 10 min (100 rpm). The cell viability was calculated by measuring the cells at a wavelength of 570 nm using a microplate reader.

Cell survival rate = (absorbance of the sample group absorbance of the normal culture control group)/absorbance of the normal culture control group ×100.

Process Optimization of siRNA Loaded Polymer Nanoparticles

Competitive Uptake Experiments of Nanoparticles

To achieve a final concentration of 50 μM, the three siRNAs were dissolved in a solution (pH 3, 10 mM pH 3) of acetate buffer. Pure water was used to dissolve the mPEG-Azo-PEI polymer and prepare a solution with a concentration of 10 mg/mL. Based on the siRNA: mPEG-Azo-PEI ratio of 1:20 (w/w), siRNA and mPEG-Azo-PEI solutions were mixed. After vortexing and mixing for 1 min, the corresponding nanoparticles were obtained by incubation at 30 °C for 1 h.

Screening of optimal composite ratio: The ratio of siRNA to PEG-Azo-PEI was varied (1:1, 1:2.5, 1:5, 1:7.5, 1:10, 1:15, 1:20, 1:25, 1:30, and 1:40), and the particle size of the composite was determined to determine the optimal ratio, wherein a minimized and stable particle preparation was selected.

Detection of the complexing ability of polymers to siRNA: A 1% agarose gel was proportionally configured to ensure equal loading for each well, and electrophoresed for 35 min at a constant pressure of 90 V in TBE buffer. After electrophoresis, a gel imager was used to visualize the electrophoretic bands, which were combined with the particle size to determine the optimal ratio of polyplexes for siRNA complexation. The experiment was repeated three times.

Table 1 Real Time Polymerase-Chain Reaction Primer Sequence

Genes	Primer Sequence-Forward	Primer Sequence-Reverse
GAPDH	GCACCGTCAAGGCTGAGAAC	CTCAAACTGATGCCCGCTTA
mettl3	TGCTTGGTTGGTGTCAAAGG	AATCTTGCGAGTGCCAGGAG

Nanoparticle Characterization

Mean Size of Nanoparticles

The mean size of nanoparticles, polydispersity index (PDI), and *Z*-potential of the polymer nanoparticles were determined using a NanoBrook 90 Plus PALS particle size analyzer.[31]

Transmission Electron Microscopic (TEM) Technique

The polymeric nanoparticle suspension was diluted to approximately 200 μg/mL using double-distilled water. One drop was placed on a copper net, stained with 2% phosphotungstic acid, and detected using TEM.[32]

Stability

Briefly, RPMI-1640 medium containing fetal bovine serum (10% and 50%) was used to dilute the siRNA-loaded polymeric nanoparticles to 10 μL. Afterwards, 0.5, 1, 2, 4, 8, 12, 24, 48, and 72 h of incubation was carried out at 37 °C before mixing the sample with loading containing 1% SDS at a ratio of 5:1. Free siRNA at the same concentration as that in the complex was diluted to 10 μL with RPMI-1640 medium and its components. After incubation at 37 °C for 0.5, 1, 2, 4, 8, 12, 24, 48, and 72 h, the samples were mixed and loaded without 1% SDS at a ratio of 5:1.

Agarose gel electrophoresis: The agarose gel (1%) was proportionally configured to ensure equal loading in each well, whereas free siRNA and mPEG-Azo-PEI@siRNA complexes were simultaneously electrophoresed in TBE buffer at a constant pressure of 90 V for 35 min. After electrophoresis, the electrophoretic bands were visualized using a gel imager, after which grayscale analysis was performed to analyze the serum stability of the free siRNA and mPEG-Azo-PEI@siRNA complexes. The experiment was repeated three times.

Experiments to Test in vitro Release of siRNA

Testing of in vitro siRNA release experiments: To maintain the sink condition, dialysis membrane bags were filled with 1 mL of mPEG-Azo-PEI@siRNA2 solution (1 mg/mL) before we tied the two ends of the membrane bags with a cotton thread. The dialysis bags were then placed in 100 mL of PBS solution (pH 7.4). To remove ethanol and exchange the buffer, the resulting dispersion was dialyzed using a 3.5 kDa MWCO membrane against PBS (pH 7.4) for 4 h, with PBS replaced every 30–60 min. At 1, 2, 3, 4, 6, 8, 12, and 24 h, we removed the release medium (1 mL) and estimated the siRNA2 content using PCR. Simultaneously, 1 mL of fresh releasing medium was added, the temperature was kept at 37 °C, and the corresponding release curve was drawn.[33]

Drug release experiment in a hypoxic environment: 1 mL of mPEG-Azo-PEI@siRNA2 solution (1 mg/mL) was placed into dialysis membrane bags, and other procedures were performed as described above. Next, we immersed the above-mentioned bags in 100 mL PBS (0.1 M, pH7.4) that comprised 100 μM NADH and 100 μg/mL NTR. Hypoxia was established by continuous N_2 purging to reduce dissolved oxygen levels. The same PBS buffer (pH 7.4) was used under both hypoxic and normoxic conditions to maintain comparable pH conditions. At the same time interval, as stated above, we removed the release medium (1 mL) and estimated the siRNA2 content using PCR. The volume of the releasing medium, maintenance at a constant temperature control, and drawing of the release curve were the same as described above.

Cumulative release rate = siRNA relative content at each time point/siRNA relative content added × 100

Competitive Uptake Experiments of Nanoparticles

Coumarin was used instead of siRNA and was loaded into the nanoparticles using the above preparation method. The logarithmic phase of HCT116 cells was inoculated into a 6-well plate (1×10^5/mL, 2 mL). The culture medium was discarded following cell adhesion. Coumarin-loaded nanoparticles were added to the cells and incubated under normal and hypoxic conditions for 0.5, 1, 2, 4, 6, 12, and 24 h, and washed three times with PBS (pH 7.4). Cells were fixed with 4% paraformaldehyde (1 mL) for 20 min. The cells were washed four times with PBS pH 7.4 for 4 times. Subsequently, nuclear staining was performed with DAPI (0.5 mL), and cells were incubated at 37 °C for 20 min. A 1mL pipette was used to drop 50 μL of anti-fluorescence quenching sealant onto the sample. Cells were viewed under a fluorescent inverted microscope, where green indicates the coumarin spectrum, and DAPI-labeled nuclei show blue light.

In vitro Antitumor Assays of the mPEG-Azo-PEI@siRNA2 Complex

MTT

The procedure for collection, digestion and centrifugation of logarithmic HCT116 cells was carried out as described in section "Selection of siRNA".

RT- PCR

Total RNA was extracted using the TRIzol reagent (Invitrogen, Carlsbad, CA). Using this kit, we reverse-transcribed RNA (1000 ng) into cDNA, followed by detection of METTL3 gene expression with RT-PCR using the corresponding kit, and GAPDH as the reference gene using the following primer sequences: forward primer sequence for the METTL3 gene was 5′TTGTCTCCAACCTTCCGTAGT 3′; reverse primer sequence was 5′CCAGATCAGAGAGGTGGTGTAG 3′; forward primer sequence for GAPDH was 5′CTGGGCTACACTGAGCACC 3′; reverse primer sequence was 5′ AAGTGGTCGTTGAGGGCAATG 3′.

Western Blot Analysis

To evaluate the protein-level expression of METTL3, Western blot analysis was performed on both HCT116 and HKF cells. Briefly, cells were seeded in 6-well plates and incubated until full adhesion. The cells were then treated with different formulations (Control and mPEG-Azo-PEI@siRNA2) under normoxic or hypoxic conditions for 48 h. After treatment, cells were washed with cold PBS and lysed using RIPA lysis buffer supplemented with protease and phosphatase inhibitors. The total protein concentration was determined using a BCA Protein Assay Kit. Equal amounts of protein samples were separated by 10% sodium dodecyl sulfate-polyacrylamide gel electrophoresis (SDS-PAGE) and subsequently transferred onto polyvinylidene fluoride (PVDF) membranes. The membranes were blocked with 5% non-fat milk in TBST for 2 h at room temperature, followed by overnight incubation at 4 °C with primary antibodies against METTL3 and GAPDH (used as the internal loading control). After washing with TBST, the membranes were incubated with HRP-conjugated secondary antibodies for 1 h at room temperature. The protein bands were visualized using an enhanced chemiluminescence (ECL) detection system.

Antitumor Assay in vivo

All animal experimental procedures were approved by the Animal Experiment Center of the Medical College of Yangzhou University (approval number: No. SYXK (Su) 2017–0044). All experiments were performed in accordance with the Chinese National Standard GB/T 35892–2018 (Guidance for the Care and Use of Laboratory Animals). For procedures requiring anesthesia, mice were anesthetized via a single intraperitoneal injection of a mixture of ketamine (100 mg/kg) and acepromazine (2.5 mg/kg), prepared in sterile physiological saline. Anesthesia depth was confirmed by the absence of a pedal reflex (toe pinch). At the experimental endpoint, euthanasia was performed under deep anesthesia by exsanguination via cardiac puncture, and cervical dislocation was performed as a secondary method of euthanasia to ensure death, in accordance with the Chinese National Standard GB/T 39760–2021 (Guidance for Euthanasia of Laboratory Animals) and the American Veterinary Medical Association (AVMA) Guidelines for the Euthanasia of Animals. Briefly, for cardiac puncture, a 22-gauge needle attached to a 1 mL syringe was inserted vertically through the sternum into the heart to withdraw blood until circulatory arrest (exsanguination). Death was confirmed by the absence of respiratory movement, cardiac activity, and corneal reflex.

Six- to eight- week- old male Balb/c nude mice (18–20 g) were obtained from the Animal Experiment Center of the Medical College of Yangzhou University. The nude mice were fed in an environment controlled at 22±1 °C, with light and dark cycles for 12h and free diet and water. The experiment was carried out one week later. A total of 30 BALB/c nude mice were randomly divided into five groups (n = 6 per group): model, positive control group (5-Fu), blank preparation (blank-mPEG-AZo-PEI), siRNA2, and mPEG-Azo-PEI-siRNA2. This study adhered to the internationally accepted standards for animal research following the 3Rs principle. The ARRIVE guidelines were used to report experiments involving live animals and to promote ethical research practices.

Establishment and Treatment of the Subcutaneous Colorectal Cancer Xenograft Model

HCT116 cells (3×10^6 cells in 100 μL PBS) were subcutaneously injected into the right axilla of nude mice to establish the xenograft model. When the tumor volume was > 15 mm^3, nude mice with well-balanced tumor growth were selected for grouping. The positive control group was given 5-Fu via intraperitoneal injection at a dose of 25 mg/kg, twice per week. Mice in groups 3, 4, and 5 were treated via tail vein administration. The dose was calculated based on the siRNA2 content (5 nmol siRNA2 per mouse per injection, approximately 3.4 mg/kg based on an average body weight of 18–20 g) and administered twice per week for two consecutive weeks (a total of four administrations), with an injection volume of 100 μL per mouse. For the treatment schedule, it was initiated on Day 1 after tumor cell inoculation, even though tumor formation generally requires several days. Treatment was started at Day 1 to evaluate the early therapeutic effects of the treatments on tumor initiation and early tumor growth, and to assess the preventive potential of the therapeutic approach. Tumor measurements were performed by an investigator blinded to group allocation.

After two weeks of continuous administration, the tumor size and body weight of the nude mice were measured on the 1^{st}, 5^{th}, 10^{th} and 15^{th} day, while a curve was drawn. On the 15^{th} day, the nude mice were dissected, and the tumors of each group were excised and weighed for pathological section analysis. Simultaneously, total RNA was extracted from the tumor tissues of mice, the expression of METTL3 at the gene level was analyzed, and the relationship between METTL3 expression and tumor changes in mice was analyzed.

Statistical Analysis

All in vitro experiments were independently repeated at least three times (biological replicates), and each experiment was performed in triplicate (technical replicates). Data are expressed as means ± standard deviation (SD). An unpaired two-tailed *t*-test was used to compare two groups. Differences between groups were analyzed using one- or two-way analysis of variance (ANOVA), followed by post-hoc tests (Dunnett's or Sidak's multiple comparison tests). Tumor volume over time was analyzed using two-way repeated-measures ANOVA (treatment × time) including the interaction term, with multiplicity-adjusted post hoc comparisons. Statistical analyses were performed using the GraphPad Prism 8 software. Differences were considered statistically significant at $P<0.05$.

Results

NMR Spectrum Analysis of mPEG-Azo-PEI

As shown in Figure 2, all key H signals in the products appeared in the H NMR spectra, wherein the key H signals of the principal materials and intermediates could be seen in the H NMR spectra of the products, thus indicating the successful preparation of mPEG-Azo-PEI.

Cytotoxicity of mPEG-Azo-PEI

The cytotoxicity assay was performed using mPEG-Azo-PEI polymer solution without siRNA loading to evaluate the intrinsic biosafety of the carrier material. At concentrations above the CMC, the polymer is expected to self-assemble into blank micellar nanostructures in aqueous media. As shown in Figure 3A, the viability of both cell types was higher than 90% at mPEG-Azo-PEI concentrations of ≤ 5 μg/mL (biological n = 3; triplicate wells per experiment). At a concentration of 10 μg/mL, the viability of the two cell types was still higher than 85%, suggesting that mPEG-Azo-PEI exhibited acceptable biosafety and low cytotoxicity in this concentration range. To further evaluate the safety profile of the complete formulation, we assessed the cytotoxicity of mPEG-Azo-PEI@siRNA2 in normal HKF cells. As shown in Figure 3B, the formulation maintained high cell viability in HKF cells even at concentrations up to 10 μg/mL, with viability remaining above 90% at the therapeutic concentration range. These results demonstrate that mPEG-Azo-PEI @siRNA2 exhibits minimal non-specific toxicity toward normal cells. In addition, compared with the lower concentration groups. The high-concentration groups showed cell death, shrinkage, rounding, and significant changes in cell morphology (Figure 3C and D).

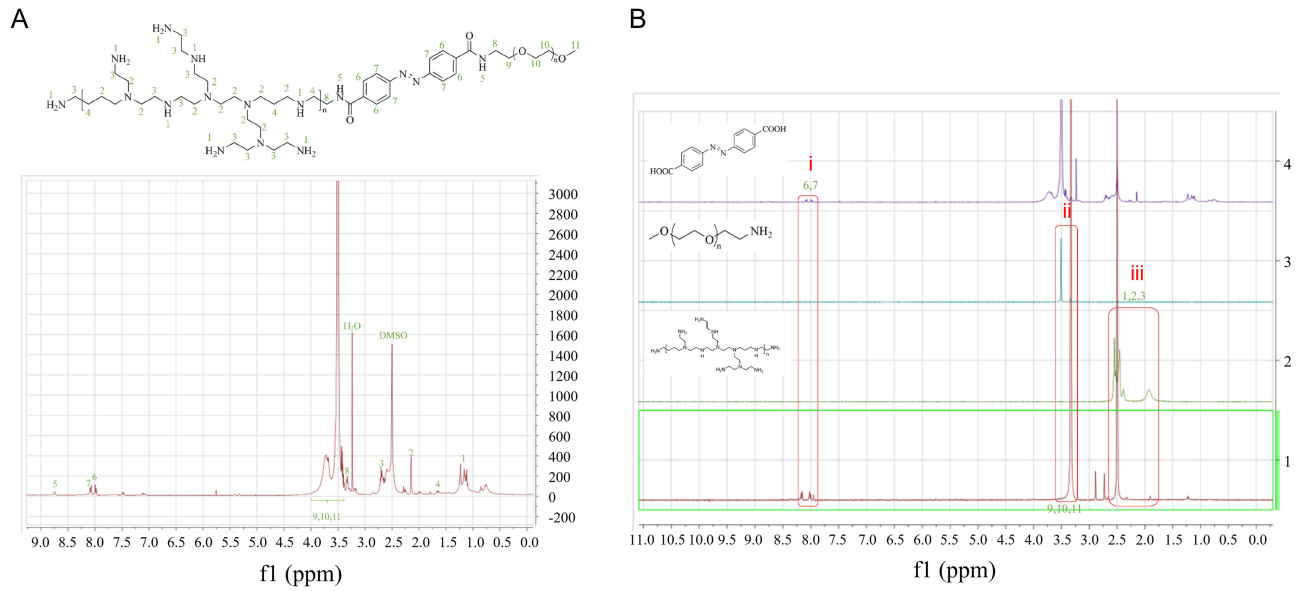

Figure 2 (**A**) ^{1}H NMR characterization of mPEG-Azo-PEI and related intermediates. (**A**) ^{1}H NMR spectrum of the final product mPEG-Azo-PEI. The numeric labels 1–11 indicate the assignments of different proton environments in the mPEG-Azo-PEI structure. Specifically, 1–5 correspond to proton signals from the PEI segment and those adjacent to the amide linkage, 6–7 correspond to the aromatic protons of the azobenzene moiety, 8–10 correspond to the methylene protons of the mPEG chain, and 11 corresponds to the terminal methoxy protons of mPEG. H_2O and DMSO represent the residual water and solvent peaks, respectively. (**B**) ^{1}H NMR spectra of key raw materials and intermediates. The different spectra are labeled 1–4 in black. The green numeric labels next to the peaks indicate the corresponding proton assignments, consistent with those shown in panel (**A**). The red boxes in panel (**B**) highlight the characteristic proton signals confirming the successful synthesis of mPEG-Azo-PEI, including (i) the aromatic protons of the azobenzene moiety (6, 7), (ii) representative proton signals of the mPEG chain (9–11), and (iii) representative proton signals of the PEI segment (1–3).

Selection of siRNA

As shown in Figure 4A–D, after siRNA2 treatment, HCT116 cells showed the lowest viability, with obvious morphological alterations observed in the representative microscopic images under the indicated culture conditions. Similarly, the relative expression of METTL3 mRNA in the cells was the lowest. Therefore, siRNA2 was selected for the subsequent experiments.

Results of Optimal Process Screening for siRNA2 Loaded Polymeric Nanoparticle

As shown in Table 2, when the ratio of siRNA2: mPEG-Azo-PEI was 1:20, the sizes of the nanoparticles and PDI of the polymer nanoparticles were small. Moreover, agarose gel electrophoresis (Figure 5A) showed that when the ratio of siRNA2 to mPEG-Azo-PEI was 1:20, no free siRNA2 was detected, indicating that all siRNA2 was complexed with mPEG-Azo-PEI.

Characterization of mPEG-Azo-PEI@siRNA2

Characterization of mPEG-Azo-PEI@siRNA2: Size, PDI, Z-Potential, TEM, EE, and DL

Particle size, PDI, and EE are important indices for evaluating the stability and uniformity of nanoparticles[34]. As shown in Figure 5B, the particle size of blank mPEG-Azo-PEI nanoparticles was 122 ± 1.21 nm, whereas that of the mPEG-Azo -PEI nanoparticles loaded with siRNA2 (mPEG-Azo-PEI@siRNA2) was 141.34 ± 2.31 nm. The PDI of mPEG-Azo-PEI @siRNA2 was 0.213 ± 0.011 with a Z-potential of +21.76 ± 1.76. Using TEM (Figure 5C), we deduced that the prepared mPEG-Azo-PEI@siRNA2 had a spherical shape with a relatively uniform distribution. The encapsulation efficiency (EE) of the mPEG-Azo-PEI@siRNA2 nanoparticles was found to be 91.23%, and the drug loading (DL) was 9.2%. The particle size was approximately 110 nm, which is consistent with the particle size assay results.

Stability

Poor self-stability and easy degradation by ribozymes in serum can lead to the reduced activity of free siRNA.[22] To verify whether the mPEG-Azo-PEI copolymer could protect free siRNA from degradation over a certain period, we examined the stability of free siRNA and the mPEG-Azo-PEI@siRNA2 complexes in media containing 10% and 50% serum. The loading containing 1% SDS used in these experiments contained a large number of anions, which

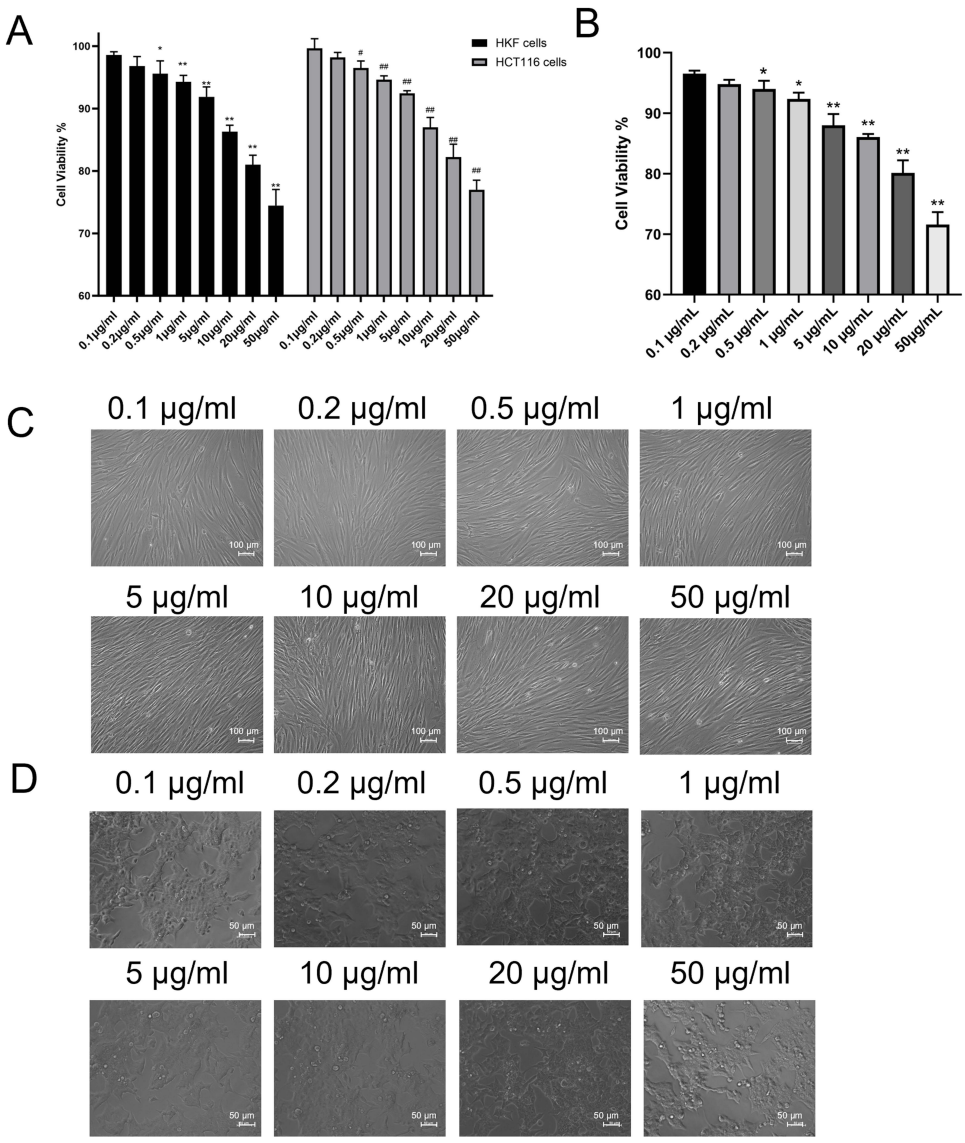

Figure 3 mPEG- Azo- PEI effect on cell viability and morphology. (**A**) Cytotoxicity assay results of mPEG-Azo-PEI on different cells; (**B**) Cytotoxicity assay results of mPEG-Azo-PEI@siRNA2 on HKF (**C**) Effects of different concentrations of mPEG-Azo-PEI on the morphological changes of HKF cells. Scale bar= 100 μm; (**D**) Effects of different concentrations of mPEG-Azo-PEI on the morphological changes of HCT116 cells. Scale bar= 50 μm. *P < 0.05, for HKF cell group compared to 0.1 μg/mL mPEG-Azo-PEI; **P < 0.01, HKF cell groups compared with 0.1 μg/mL mPEG-Azo-PEI; #P < 0.05, for HCT116 cell group compared to 0.1 μg/mL mPEG-Azo-PEI; ##P < 0.01, for HCT116 cell group compared to 0.1 μg/mL mPEG-Azo-PEI. Biological n = 3; triplicate wells per experiment.

disrupted the electrostatic interaction of mPEG-Azo-PEI with siRNA2 and dissociated the siRNA from mPEG-Azo-PEI@siRNA2. Hence, the change in band intensity can be detected by gel electrophoresis. As shown in Figures 6A and B, the free siRNA could only be stably stored for 4 h in the medium containing 10% and 50% serum, while the siRNA band of mPEG-Azo-PEI@siRNA2 could still be detected after 72 h of incubation in the medium containing 10% and 50% serum, thus indicating that the mPEG-Azo-PEI copolymer had strong complexation ability with siRNA2 and good stability.

Cumulative Release Rate in vitro

As shown in Figure 6C, the cumulative release of siRNA2 within 24 h in a normal environment was approximately 10%, which was far less than 95% of that in a hypoxic environment. Statistically, this significant difference illustrated that the nanoparticles prepared with this hypoxia-sensitive polymer were better and capable of degrading and accelerating drug release in an anoxic environment.

https://doi.org/10.2147/IJN.S588018

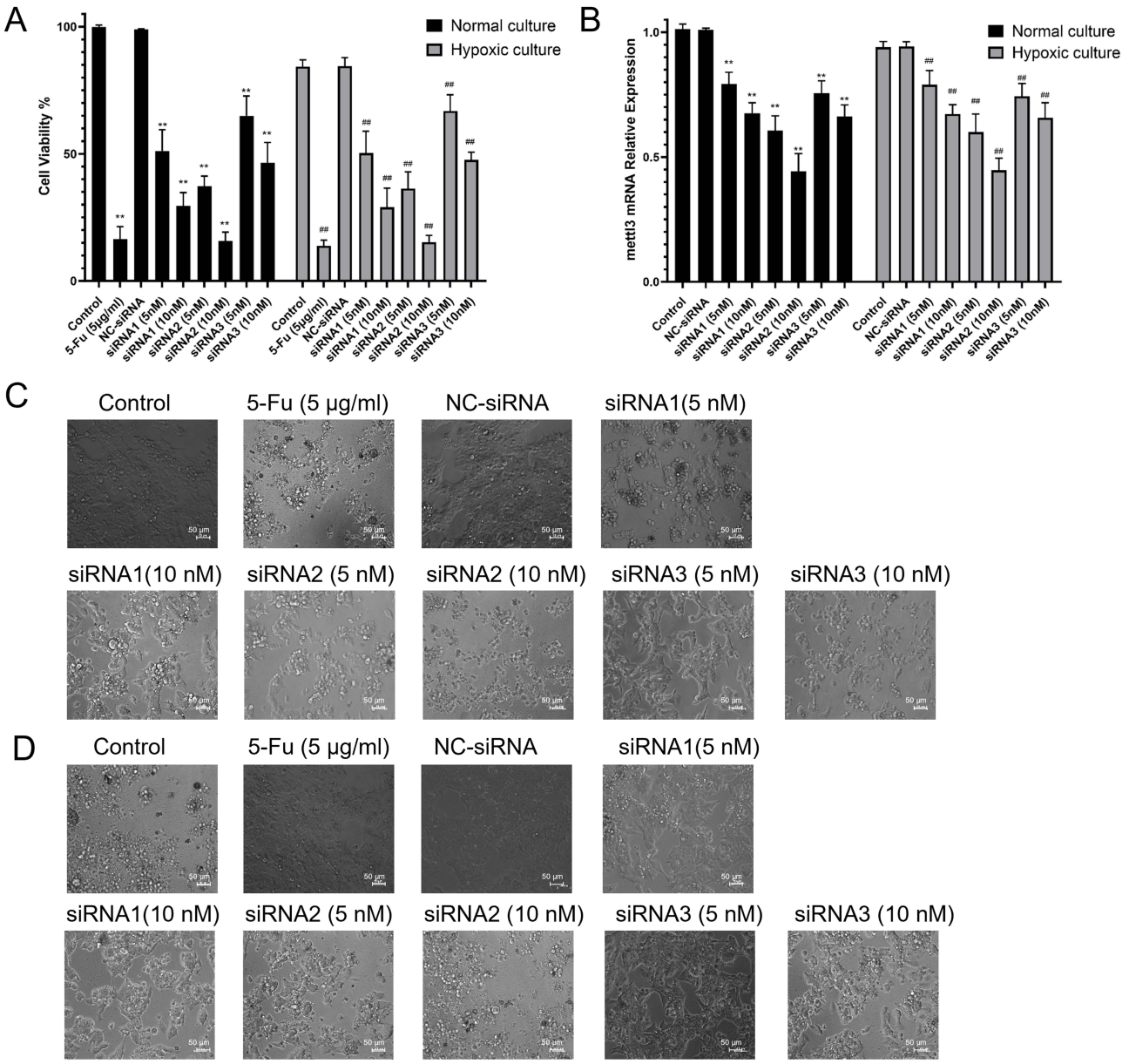

Figure 4 Effects of the three siRNAs on cell viability and relative expression of mettl3 mRNA in HCT116 cells under different culturing conditions. (**A**) HCT116 cells viability under different culturing conditions; (**B**) Relative expression of mettl3 mRNA in HCT116 cells; (**C**) Morphological changes of cells under normal culture conditions. Scale bar= 50 μm; (**D**) Morphological changes of cells under hypoxic culture conditions. Scale bar= 50 μm. **P< 0.01, under normal culturing conditions, comparable to control group; ##P< 0.01, under hypoxic culturing conditions, comparable to control group. Biological n = 3; triplicate wells per experiment.

Cell Uptake Experiments of Nanoparticles

As shown in Figure 7A and B, both normal and anoxic cultures showed that coumarin-loaded nanoparticles could be taken up by HCT116 cells, which changed over time. The maximum fluorescence intensity was obtained after 4 h of incubation,

Table 2 Particle Size (PS) and Polydispersity Index (PDI) of Polymeric Nanoparticle Fabricated in Distinct Ratios

Ratio	1:1	1:2.5	1:5	1:7.5	1:10	1:15	1:20	1:25	1:30	1:40
PS	183.75 ±5.43	177.37 ±5.28	162.73 ±4.18	161.739 ±4.28	155.28 ±4.18	152.38 ±3.28	141.34 ±2.31	138.23 ±2.87	135.38 ±1.87	132.82 ±1.72
PDI	0.293 ±0.031	0.287 ±0.024	0.254 ±0.019	0.265 ±0.031	0.252 ±0.024	0.254 ±0.027	0.213 ±0.011	0.204 ±0.009	0.210 ±0.012	0.198 ±0.015

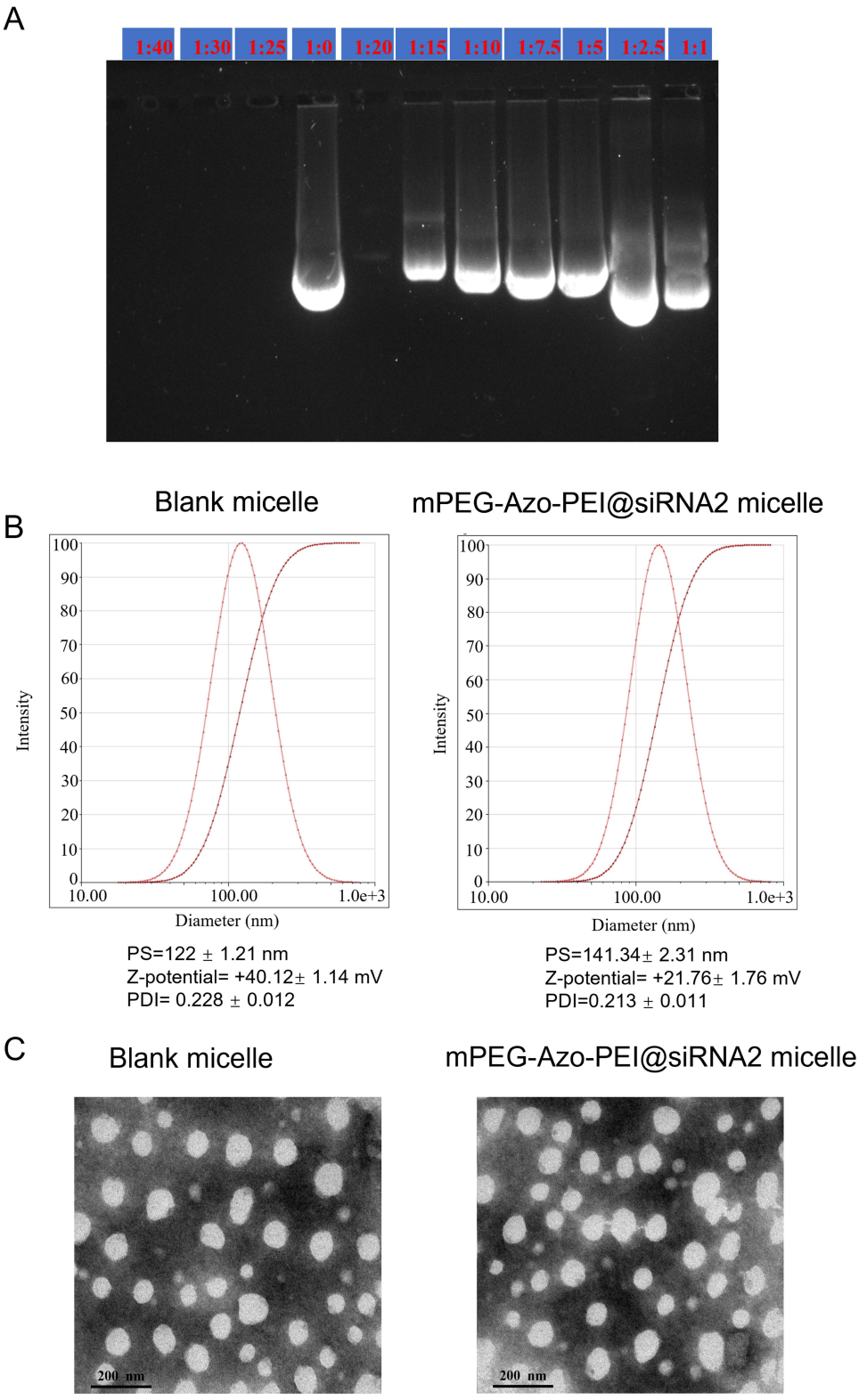

Figure 5 Characterization of mPEG-Azo-PEI@siRNA2 Nanoparticles. (**A**) Complexation ability of mPEG-Azo-PEI with siRNA2; (**B**) Particle size (PS) profiles of blank and mPEG-Azo-PEI@siRNA2 nanoparticles; (**C**) TEM images of blank and mPEG-Azo-PEI@siRNA2 nanoparticles.

https://doi.org/10.2147/IJN.S588018

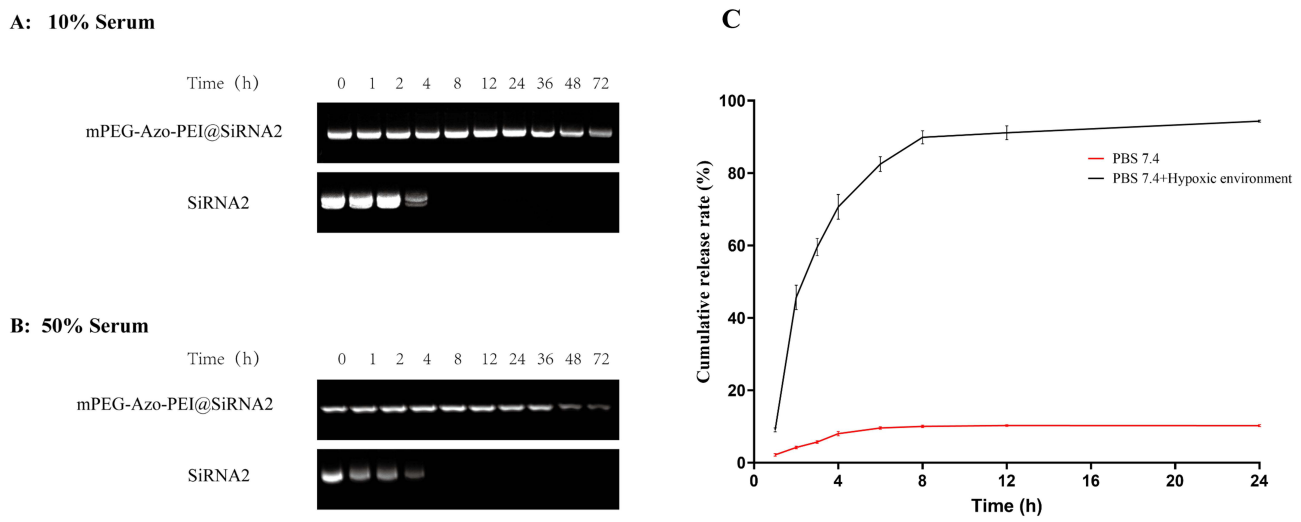

Figure 6 Results of stability inspection of mPEG-Azo-PEI@siRNA2 (**A** and **B**) and cumulative release results of siRNA2 in different environments (**C**).

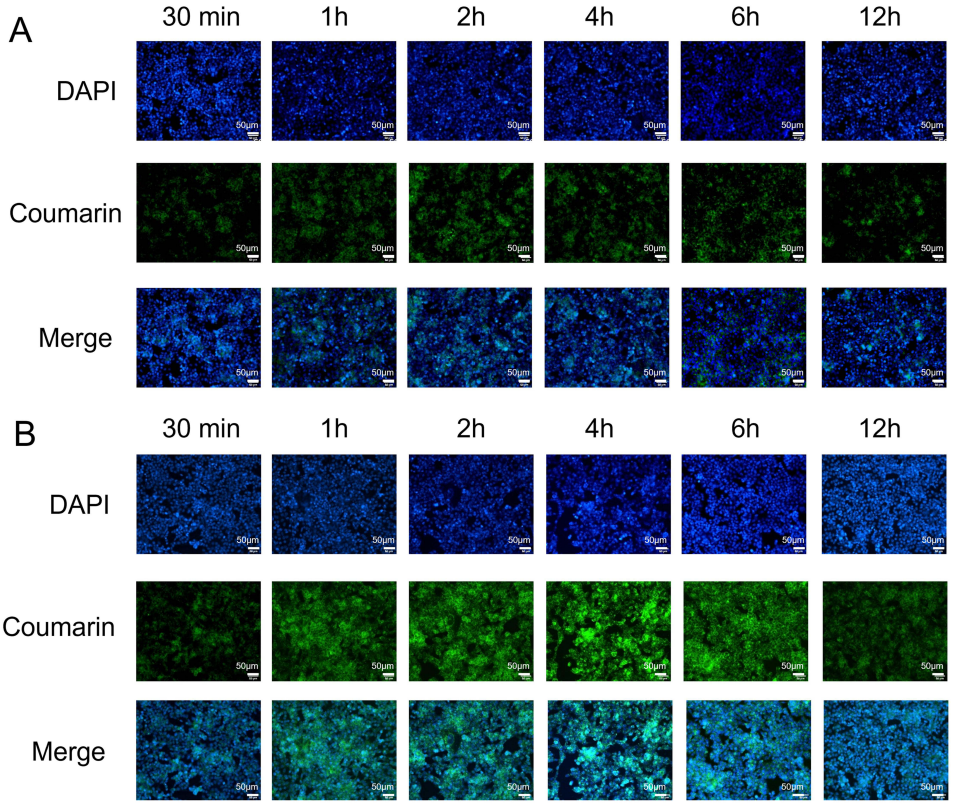

Figure 7 Real-time fluorescent inverted microscope images of cellular uptake of coumarin nanoparticles under normal culturing conditions (**A**) and hypoxic culturing conditions (**B**). (20×, scale = 50 μm).

indicating maximum cell intake at this time point. Moreover, fluorescence intensity was significantly enhanced under anaerobic conditions at each time point, indicating that the intake of coumarin-loaded nanoparticles by HCT116 cells was higher under anaerobic conditions, which was conducive to drug uptake in the anoxic environment in vivo.

In vitro Antitumor Results

As shown in Figure 8A, the preparations effectively inhibited the proliferation of HCT116 cells under both normal culture and hypoxic culture conditions. Representative microscopic images in Figures 8B–E qualitatively suggested treatment-associated morphological changes, which appeared more pronounced under hypoxic culture conditions at the same concentration. Compared with normal culture conditions, cell viability was significantly lower under hypoxic culture conditions ($P < 0.01$). As shown in Figure 8F, the IC50 values of the preparations from normal and hypoxic cultures were 1.133 and 0.481 nM, respectively, whereas the respective IC50 values of the raw material from normal and hypoxic cultures were 3.174 and 1.638 nM, respectively. Moreover, mPEG-Azo-PEI@siRNA2 effectively inhibited the mRNA expression of METTL3 gene under both normal and hypoxic culture conditions, and the effect was more prominent under hypoxic conditions at the same concentration (Figure 8G). Treatment with mPEG-Azo-PEI@siRNA2 successfully and significantly downregulated the METTL3 protein level in HCT116 cells (Figure 8H). Importantly, the METTL3 expression in normal HKF cells remained unaffected by the identical treatment. The uncropped original Western blot images of METTL3 and GAPDH in HCT116 and HKF cells are provided in Supplementary Figure 1. These findings provide robust evidence that our engineered hypoxia-sensitive nanoparticles can achieve sequence-specific gene silencing and exhibit selective toxicity toward cancer cells without disrupting the basal METTL3 functions in normal tissues. Taken together, these results indicate that, at the same concentration, the preparations exerted a stronger in vitro antitumor effect under hypoxic culture conditions than under normal culture conditions.

Antitumor Assay in vivo

The Body Weight and Tumor Volume and Tumor Weight of Mice

In vivo data were obtained from BALB/c nude mice (n=6 per group). As shown in Figure 9A, after 2 weeks of treatment, the body weight of mice in the 5-FU group was significantly lower than that in the model group ($P < 0.01$), but the body weights of mice in the siRNA2 and mPEG-Azo-PEI-siRNA2 groups substantially increased ($P < 0.01$), amid the body weight of mice in the mPEG-Azo-PEI-siRNA2 group being markedly higher than that of the siRNA2 group ($P < 0.01$).

Based on the tumor weight and volume change diagram of mice (Figure 9B–D), appropriate statistical comparison with the model group showed that the aforementioned variables decreased substantially ($P < 0.01$) in mice that were allotted to the positive group, siRNA2, and mPEG-Azo-PEI-siRNA2 groups, thus indicating that 5-FU and siRNA2 can effectively inhibit tumor growth in mice. Likewise, comparison with the siRNA2 group led to the observation of smaller tumor weight and tumor volume in the mPEG-Azo-PEI-siRNA2 group mice, coupled with a marked ($P < 0.01$) tumor inhibition effect, which indicates that mPEG-Azo-PEI as a carrier material could effectively deliver siRNA2 to the tumor site and enhance the antitumor effect of the drug.

Analysis of HE Results

As shown in Figure 9E, the tumor tissue cells in the model group were relatively densely arranged, with large and numerous nuclei, indicating that the tumor cells grew vigorously and were in good condition, while nuclear staining was clearly visible. The results for the tumor tissue sections in the blank preparation group were consistent with those in the model group. The treatment groups (b, d, and e) showed necrotic areas in the tumor tissue, loose tumor tissue, decreased number of nuclei, and an irregular arrangement of cells. Necrosis of tumor cells in groups b and e was the most obvious. These results indicate that siRNA2 and mPEG-Azo-PEI-siRNA2 can effectively inhibit tumor growth.

Results of PCR

The results of PCR (Figure 9F) showed that the relative expression level of METTL3 at the RNA level in the model and blank preparation groups were high, while the treatment group could significantly reduce the relative expression levels of METTL3 at the RNA level ($P < 0.01$). Compared to the siRNA2 group, the mPEG-Azo-PEI-siRNA2 group mice had a greater reduction in the relative expression of METTL3 at the RNA level ($P < 0.01$). These results were consistent with the tumor size, volume, and HE test results.

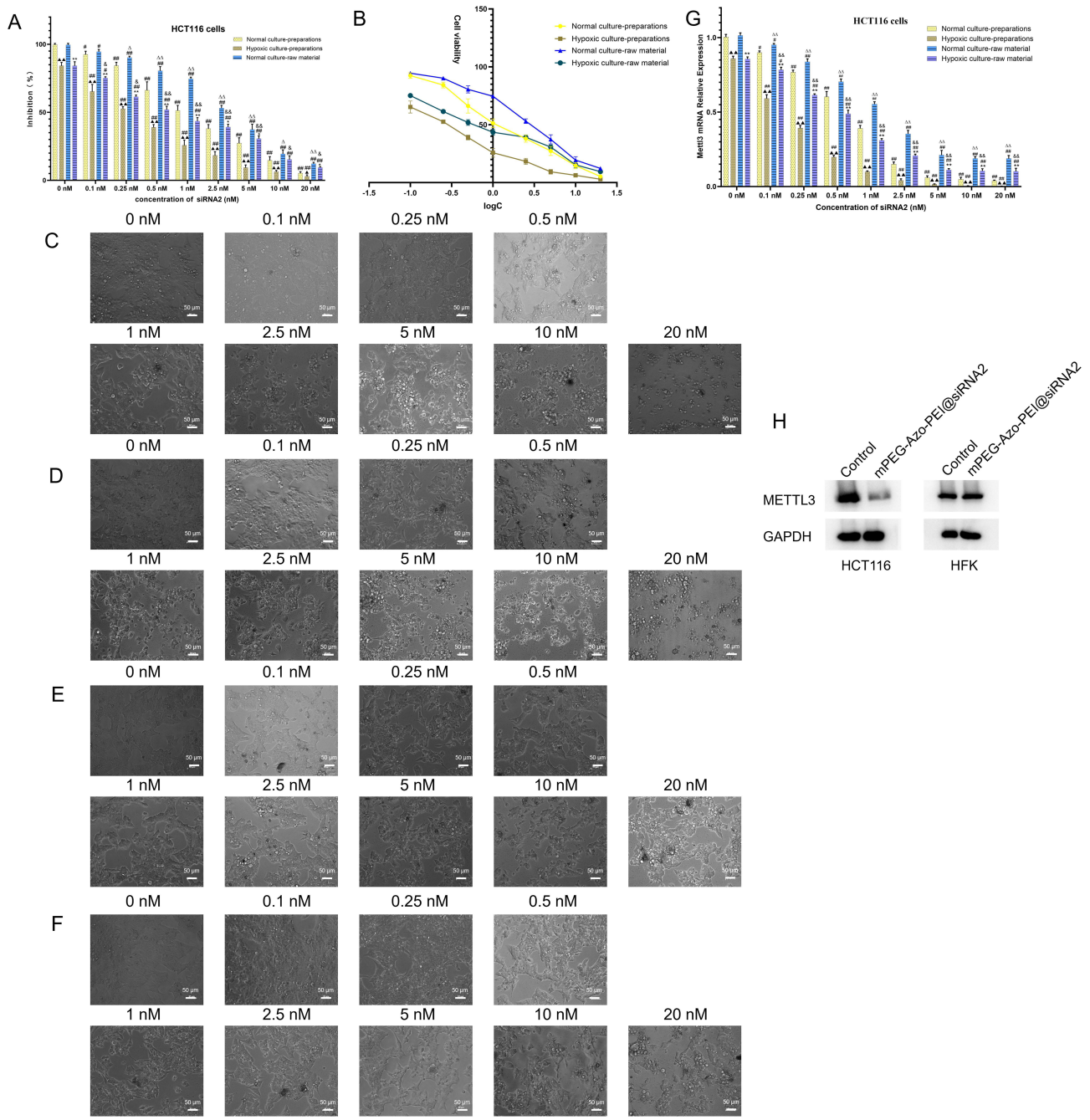

Figure 8 Effects of mPEG-Azo-PEI@siRNA2 on the activity of HCT116 cells and METTL3 relative mRNA expression. The results of the mPEG-Azo-PEI@siRNA2 MTT assay in two environments (**A**); IC50 results of mPEG-Azo-PEI@siRNA2 under normal and hypoxic culture conditions (**B**); Morphological changes of cells under normal culture of preparations (**C**), hypoxic culture of preparations (**D**), normal culture of raw material (**E**) and hypoxic culture of raw material (**F**); The relative expression of mettl3 gene detected by RT-PCR under different concentration of siRNA2 (**G**); Representative immunoblot of METTL3 in HCT116 and HKF cells (**H**). (#P< 0.05 and ##P< 0.01, inhibition rate of different concentrations of siRNA2 in each group compared to inhibition rate of siRNA2 at 0 nM; ▲P< 0.05 and ▲▲P< 0.01, preparations under normal conditions compared to those with the same siRNA2 concentration under hypoxic conditions; *P< 0.05 and **P< 0.01, raw materials under normal conditions compared to raw materials with the same concentration of siRNA2 under hypoxia; ΔP< 0.05 and ΔΔP< 0.01, preparations with the same concentration of siRNA2 under normal culture conditions compared with raw materials; andP< 0.05 and andandP< 0.01, preparations with the same concentration of siRNA2 under hypoxic culture conditions compared with raw materials). Biological n = 3; triplicate wells per experiment.

Discussion

Worldwide morbidity and mortality data on cancer of colon-rectum depict an increasing trend, and it is considered the third most widespread carcinoma.[35] Chemotherapy is greatly affected by chemoresistance, which is a common malignancy of the gastro-intestinal tract, chemotherapy of the disease is greatly affected by chemoresistance.[36] The ability of

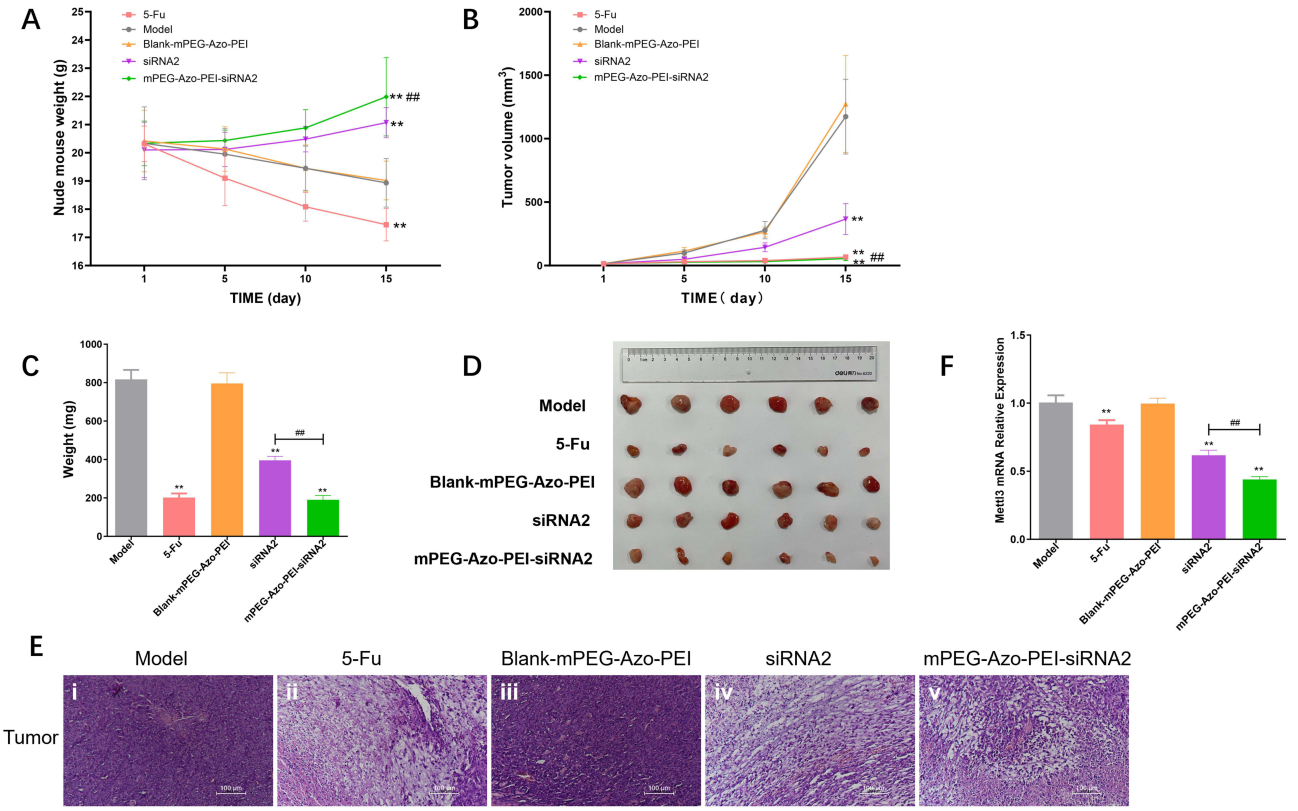

Figure 9 Changes in body weight, tumor volume, and histopathological analysis of mice after 14 days of treatment. (**A**) Line chart of changes in body weight; (**B**) Line chart of tumor volume; (**C**) Tumor weight; (**D**) Physical appearance of tumors; (**E**) Histopathological analysis of tumors: (i) model group, (ii) 5-Fu group, (iii) blank-mPEG-Azo-PEI group, (iv) siRNA2 group, (v) mPEG-Azo-PEI-siRNA2 group. Scale bar= 100 μm; (**F**) Relative expression of METTL3 at the RNA level (n = 6 mice per group; **: compared with the model group, P < 0.01; ##: compared with the siRNA2 group, P < 0.01). Tumor volume over time was analyzed using two-way repeated-measures ANOVA (treatment × time) including the interaction term, with multiplicity-adjusted post hoc comparisons.

cancer cells of the colon and rectum to adapt to hypoxic conditions has been shown to cause chemoresistance.[37] In addition, the suppression of METTL3 expression in cancer cells of the colon rectum has been shown to be key in the treatment of this disease.[16] Based on the existing literature, we designed and fabricated mPEG-Azo-PEI, which self-assembles into nanoparticles via micellar self-assembly. Wherein the Azo moiety was hypoxia-sensitive, with the potential to increase the silencing effect of METTL3 siRNAs under hypoxic conditions in tumor cells. As self-assembling nanoparticles comprising amphipathic molecules, nanoparticles are popular because they can potentially incorporate and deliver drugs in various forms, including siRNAs, wherein they increase the delivery of such payloads to tumor sites. To successfully fabricate mPEG-Azo-PEI, we examined the appearance of key H signals in the principal materials and intermediates of the nanoparticle. The H NMR was selected for this purpose because it has been applied to preliminarily identify the molecular structures of similar materials. Corroboratively, Kang et al utilized H NMR to ascertain the structure of a delivery system developed for siRNA (bPEI1.8k-C6-NI).[38]

CMC was estimated to confirm the self-assembly potential of mPEG-Azo-PEI in aqueous solution. The CMC of mPEG-Azo-PEI was determined to be 0.001687 mg/mL, indicating strong self-assembly capability and favorable stability under dilution conditions. The low CMC value is consistent with the formation of amphiphilic micellar nanostructures, in which hydrophilic mPEG chains are oriented toward the aqueous phase, while hydrophobic Azo segments are preferentially located within the nanoparticle core. With regard to the biosafety and toxicity of mPEG-Azo-PEI, we observed that the viability of both cell types was higher than 90% at mPEG-Azo-PEI concentrations of ≤ 5 μg/mL (Figure 3A). Even when the polymer concentration was increased to 10 μg/mL, we still observed the viability of the two cell types remained higher than 85%. These observations suggest that the mPEG-Azo-PEI material demonstrated better biosafety and less cytotoxicity within this concentration range. One of the major drawbacks of antitumor

https://doi.org/10.2147/IJN.S588018

chemotherapies is their deleterious side effects on normal cells; hence, the identification of alternative materials with minimal adverse effects for antitumor drugs has become paramount in clinical settings.

After confirming that mPEG-Azo-PEI is biosafe and less cytotoxic, we selected siRNA to be encapsulated in the aforementioned carrier. Based on their effect on HCT116 cells, we chose siRNA2, which suppresses the growth of HCT116 cells and the expression of METTL3 mRNA in these cells. Notably, siRNA2 has been found to suppress metastasis of cancer to the colon and rectum, which may explain the above observation.[39] Based on the ratio and agarose gel electrophoresis results, we optimally formed mPEG-Azo-PEI@siRNA2 at a siRNA2: mPEG-Azo-PEI ratio of 1:20, coupled with full incorporation of siRNA2 into mPEG-Azo-PEI, wherein the size and PDI of the optimized nanoparticles were smaller. Physical characterization of the nanoparticle was performed, wherein we discovered the respective size of particles, PDI and Z-potential to be 141.34 ± 2.31 nm, 0.213 ± 0.011 and +21.76 ± 1.76 (Figure 5B). The presence of a positive charge in the nanoparticles may be ascribed to PEI, which is a cationic polymer that has been used as a gene carrier in many studies.[40] The nanoparticles exhibited a moderately positive zeta potential, which may facilitate cellular uptake via electrostatic interactions with negatively charged cell membranes. However, it is acknowledged that highly positive surface charge may increase nonspecific protein adsorption and potential cytotoxicity in vivo. In this system, the PEGylated structure of mPEG-Azo-PEI may partially shield the surface charge, thereby reducing nonspecific interactions and improving circulation stability. Moreover, the minimal cytotoxicity observed in vitro and the stable body weight of treated mice suggest acceptable biocompatibility within the investigated dosage range. The available literature suggests that nanoparticles <200 nm are capable of evading mono-nuclear phagocytic-scavenging with the potential to passively target tumors via increased permeation and retention.[41,42]

It is well known that nanoparticles with favorable stability can prolong the circulation of drugs in the bloodstream, with concomitant targeted accumulation at tumor sites.[43] Consistent with this assertion, we confirmed that our nanoparticles might protect free siRNA from degradation over a certain period, wherein we discovered that the mPEG-Azo-PEI copolymer demonstrated good stability and potential complexation with siRNA2. Hence, our carrier may protect free siRNA2 from degradation during circulation in the bloodstream.

The in vitro release of drugs is important for simulating the in vivo conditions. Therefore, we assessed the release of free siRNA2 from mPEG-Azo-PEI@siRNA2 under both normal and hypoxic conditions. Within 24 h of observation, the cumulative release of siRNA2 (Figure 6C) in a normal environment was paltry 10%, amid was far less than 95%, comparable to the hypoxic environment. The underlying reason for this observation may be that the nanoparticle prepared with a hypoxia-sensitive polymer (Azo) was better and capable of degrading and accelerating drug release in an anoxic environment. Usually, in a hypoxic tumor environment, azo reductase catalyzes the degradation of Azo with nicotinamide adenine dinucleotide phosphate (NADPH) as the coenzyme after mPEG-Azo-PEI@siRNA2 penetrates the tumor tissue.[44,45]

Usually, the process of human disease development is reproduced during research with the aid of cell cultures and modeled animals.[46] Hence, we used HCT116 cells and a tumor-bearing BALB/c nude mouse model to reproduce the process of colorectal tumor development. For the cell culturing study, we selected HCT116 cells because the existing literature has established that these cells demonstrate invasiveness and high motility during in vitro experimentations.[47] In addition, based on the notion that tumors of the colon and rectum are similar, we modeled rectal tumors in mice to study CRC.[48]

After modeling, we measured the tumor weight, volume, and body weight of the mice to ascertain their responses to treatment,[49] wherein Dosage forms such as 5-FU, siRNA, and mPEG-Azo-PEI@siRNA2 markedly reduced the aforementioned variables, suggesting that they have the potential to suppress the growth of colorectal tumors (Figure 9). In addition, as can be seen from the body weight curve of the mice (Figure 9A), after two weeks of treatment, we observed that the body mass of mice in the 5-FU group was significantly reduced compared to that of the model group, but those of mice in the siRNA2 and mPEG-Azo-PEI-siRNA2 groups substantially increased. This observation corroborates the existing theory that the body weight of patients with colorectal tumors varies during treatment.[50] In addition, the reduction in body weight by 5-FU agrees with the findings of earlier studies by Tao et al[51,52] The pronounced loss of body weight in mice that received 5-FU may be ascribed to the adverse effects of the drugs, including increased loss of appetite and decreased intake of foods.[53] However, the observed increase in body weight of mice administered siRNA2

and mPEG-Azo-PEI-siRNA2 suggests a positive response to treatment. Corroboratively, available work has established an increase in body weight among patients with colon cancer who underwent adjuvant chemotherapy.[54,55] Currently, the underlying reason for this observation is not yet known, but it may be the metabolic and physiological changes that occur during treatment.

As a type of solid tumor, CRC exhibits a hypoxic microenvironment, which in turn promotes rapid tumor growth to outmatch the supply of oxygen, thus contributing to the aforementioned condition.[27] Therefore, we sought to utilize hypoxic conditions to treat cancers of the colon and rectum. In the present study, under both normal and hypoxic culture conditions, mPEG-Azo-PEI@siRNA2 effectively inhibited the proliferation of HCT116 cells and the relative mRNA expression of METTL3 (Figure 8A and G); however, the effect of the same concentration of mPEG-Azo-PEI@siRNA2 was more prominent in hypoxic environments. Collectively, the in vitro antitumor effects of the same concentration of mPEG-Azo-PEI@siRNA2 were stronger under hypoxic conditions. Thus, the hypoxia-enhanced efficacy suggests that this platform may be particularly suitable for targeting hypoxic tumor subregions that are often associated with aggressive behavior and reduced chemotherapy sensitivity, where triggered release could improve local gene silencing and potentially counter hypoxia-driven resistance.[56] Similarly, the in vivo application of mPEG-Azo-PEI@siRNA2 in the aforementioned rectal mouse model showed that mPEG-Azo-PEI as a carrier material could effectively deliver siRNA2 to the tumor site and enhance the antitumor effect of the drug. The enhanced antitumor activity of mPEG-Azo-PEI @siRNA2 can be attributed to its ability to self-assemble into nanoparticles, coupled with increased stability and hypoxia-induced degradation to effectively release siRNA2 at the rectal tumor site.[38] However, although mPEG-Azo-PEI@siRNA2 showed improved in vivo efficacy compared with free siRNA, it did not completely eliminate the tumors. This may be explained by several factors beyond delivery efficiency. First, tumor hypoxia is spatially heterogeneous, and the extent of hypoxia can vary across different tumor regions; therefore, activation of the hypoxia-responsive Azo linker and subsequent siRNA release may be non-uniform, leaving normoxic or less-hypoxic areas insufficiently exposed to effective siRNA levels.[57] Second, as a solid tumor, colorectal/rectal tumors often exhibit high interstitial fluid pressure and poor vascularization, which can limit nanoparticle extravasation and restrict penetration into deeper tumor tissue, thereby reducing the overall distribution of siRNA throughout the tumor mass.[58] Third, METTL3 silencing may lead to adaptive activation of survival pathways that partially sustain tumor growth and survival, suggesting that dual targeting of METTL3 and the JAK1/STAT3 axis (eg., p-STAT3 inhibition) may offer potential therapeutic avenues for colorectal cancer.[59]

While the present study demonstrates that the hypoxia-responsive mPEG-Azo-PEI platform can enhance siRNA delivery and improve antitumor efficacy, several limitations warrant consideration. First, the in vivo validation was restricted to a subcutaneous xenograft mouse model, which may not fully capture the inter- and intra-tumoral heterogeneity observed in colorectal/rectal cancer. Future studies should extend evaluation to more clinically relevant settings, including orthotopic models and patient-derived xenografts. Moreover, to interrogate immune-related effects, immunocompetent syngeneic models will be required. Second, METTL3 silencing was confirmed at the transcript level; however, protein-level validation and systematic characterization of downstream signaling alterations were not performed. Follow-up work should quantify METTL3 protein expression and map pathway-level consequences, with particular attention to the JAK/STAT3 axis and potential compensatory programs that may attenuate durable responses. Third, immune consequences were not assessed in the current work. Given the established interplay between hypoxia, the tumor microenvironment, and therapeutic responsiveness, future investigations should incorporate immune profiling (eg., immune-cell infiltration and cytokine signatures) to evaluate whether the treatment modulates antitumor immunity or inflammatory status. Additionally, the current study lacks an in vivo control group treated with nanoparticles loaded with scrambled or non-specific siRNA. While our blank carrier demonstrated good biocompatibility, the absence of this specific control limits our ability to completely rule out potential off-target effects or systemic immune stimulation induced by the nanoparticle-RNA complex itself, which should be rigorously evaluated in future preclinical toxicological studies. Finally, although in vitro cytotoxicity and the absence of overt body-weight loss in vivo suggest acceptable tolerability within the tested dose range, comprehensive safety evaluation remains necessary for translational development. Future studies should therefore include hematology, serum biochemistry, and histopathological examination of major organs to more rigorously define systemic toxicity and off-target risk.

Conclusion

Hypoxia-sensitive mPEG-Azo-PEI@siRNA2 nanoparticles were successfully prepared for the first time. The polymeric nanoparticles exhibited good biosafety, small particle size, and favorable stability, and enabled hypoxia-activated (hypoxia-responsive) siRNA release, with a cumulative release rate of more than 95% under hypoxic conditions. In vitro and in vivo antitumor experiments further demonstrated that the inhibitory effect on tumor cell proliferation was prominent under hypoxic conditions. Although the nanoparticle formulation significantly suppressed tumor growth compared with the model group and the free siRNA group, complete tumor regression was not achieved, indicating opportunities for further optimization. Such optimization may include exploring higher or more frequent dosing regimens, combination strategies with standard therapies, or further engineering the carrier to improve penetration into dense tumor regions. Therefore, this polymeric nanoparticle platform represents a promising hypoxia-activated targeting strategy for colorectal cancer therapy and warrants further validation in more clinically relevant models.

Abbreviations

WTAP, Wilms tumor-1-associated protein; METTL3 and METTL14, methyl-transferase-like protein-3 and-14; EMT, epithelial-mesenchymal transition; HCT116, Human Colon Tumor Cell Line 116; 5-Fu, 5-fluorouracil; GAPDH, glyceraldehyde-3-phosphate dehydrogenase; PDI, polydisperse index; TEM, Transmission electron microscopy; SD, standard deviation; NADPH, nicotinamide adenine dinucleotide phosphate; RT-PCR, real-time polymerase chain reaction; siRNA, small interfering RNA; MTT, 3-(4,5-dimethylthiazol-2-yl)-2,5-diphenyltetrazolium bromide; PBS, Phosphate-buffered saline; DAPI, 4',6-diamidino-2-phenylindole; DMEM, Dulbecco's modified eagle medium; RPMI-1640: roswell park memorial institute 1640 Medium.

Acknowledgments

The authors greatly appreciate the contributions of all authors. This paper has been uploaded to SSRN as a preprint: https://papers.ssrn.com/sol3/papers.cfm?abstract_id=5388397.

Funding

This work was supported by Research General Project of Yangzhou Municipal Health Commission (Project No: 2023-2-17).

Disclosure

The authors report no conflicts of interest in this work.

References

1. Pan J, Xie Y, Li H, et al. mmu-lncRNA 121686/hsa-lncRNA 520657 induced by METTL3 drive the progression of AKI by targeting miR-328-5p/HtrA3 signaling axis. *Mol Ther*. 2022;30(12):3694–3713. doi:10.1016/j.ymthe.2022.07.014
2. An Y, Duan H. The role of m6A RNA methylation in cancer metabolism. *Mol Cancer*. 2022;21(1):14. doi:10.1186/s12943-022-01500-4
3. Chen T, Hao YJ, Zhang Y, et al. m(6)A RNA methylation is regulated by MicroRNAs and promotes reprogramming to pluripotency. *Cell Stem Cell*. 2015;16(3):289–301. doi:10.1016/j.stem.2015.01.016
4. Batista PJ, Molinie B, Wang J, et al. m(6)A RNA modification controls cell fate transition in mammalian embryonic stem cells. *Cell Stem Cell*. 2014;15(6):707–719. doi:10.1016/j.stem.2014.09.019
5. Dominissini D, Moshitch-Moshkovitz S, Schwartz S, et al. Topology of the human and mouse m(6)A RNA methylomes revealed by m(6)A-seq. *Nature*. 2012;485(7397):201–U84. doi:10.1038/nature11112
6. Meyer KD, Saletore Y, Zumbo P, et al. Comprehensive analysis of mRNA methylation reveals enrichment in 3 'UTRS and near stop codons. *Cell*. 2012;149(7):1635–1646. doi:10.1016/j.cell.2012.05.003
7. Ma S, Chen C, Ji X, et al. The interplay between m6A RNA methylation and noncoding RNA in cancer. *J Hematol Oncol*. 2019;12(1):121. doi:10.1186/s13045-019-0805-7
8. Deng LJ, Deng WQ, Fan SR, et al. m6A modification: recent advances, anticancer targeted drug discovery and beyond. *Mol Cancer*. 2022;21(1):52. doi:10.1186/s12943-022-01510-2
9. Lan Q, Liu PY, Bell JL, et al. The emerging roles of RNA m(6)A methylation and demethylation as critical regulators of tumorigenesis, drug sensitivity, and resistance. *Cancer Res*. 2021;81(13):3431–3440. doi:10.1158/0008-5472.CAN-20-4107
10. Zaccara S, Ries RJ, Jaffrey SR. Reading, writing and erasing mRNA methylation. *Nat Rev Mol Cell Biol*. 2019;20(10):608–624. doi:10.1038/s41580-019-0168-5

11. Liu J, Yue Y, Han D, et al. A METTL3-METTL14 complex mediates mammalian nuclear RNA N-6-adenosine methylation. *Nat Chem Biol*. 2014;10(2):93–95. doi:10.1038/nchembio.1432
12. Brabletz S, Schuhwerk H, Brabletz T, et al. Dynamic EMT: a multi-tool for tumor progression. *EMBO J*. 2021;40(18):e108647. doi:10.15252/embj.2021108647
13. Ashrafizadeh M, Mirzaei S, Hashemi F, et al. New insight towards development of paclitaxel and docetaxel resistance in cancer cells: EMT as a novel molecular mechanism and therapeutic possibilities. *Biomed Pharmacother*. 2021;141:111824. doi:10.1016/j.biopha.2021.111824
14. Pan J, Liu F, Xiao X, et al. METTL3 promotes colorectal carcinoma progression by regulating the m6A–CRB3–Hippo axis. *J Exp Clin Cancer Res*. 2022;41:19. doi:10.1186/s13046-021-02227-8
15. Sun Y, Gong W, Zhang S, et al. METTL3 promotes colorectal cancer progression through activating JAK1/STAT3 signaling pathway. *Cell Death Dis*. 2023;14:765. doi:10.1038/s41419-023-06287-w
16. Chen H, Pan Y, Zhou Q, et al. METTL3 inhibits antitumor immunity by targeting m6A-BHLHE41-CXCL1/CXCR2 axis to promote colorectal cancer. *Gastroenterology*. 2022;163(4):891–907. doi:10.1053/j.gastro.2022.06.024
17. Li M, Xia M, Zhang Z, et al. METTL3 antagonizes 5-FU chemotherapy and confers drug resistance in colorectal carcinoma. *Int J Oncol*. 2022;61:106. doi:10.3892/ijo.2022.5396
18. Ma S, Zhang J, Yan T, et al. Novel strategies to reverse chemoresistance in colorectal cancer. *Cancer Med*. 2023;12(10):1. doi:10.1002/cam4.5594
19. Lan Q, Liu PY, Haase J, et al. The critical role of RNA m(6)A methylation in cancer. *Cancer Res*. 2019;79(7):1285–1292. doi:10.1158/0008-5472.CAN-18-2965
20. Li F, Wang H, Huang H, et al. m6A RNA methylation regulators participate in the malignant progression and have clinical prognostic value in lung adenocarcinoma. *Front Genet*. 2020;11:994. doi:10.3389/fgene.2020.00994
21. Pan F, Lin XR, Hao LP, et al. The role of RNA methyltransferase METTL3 in hepatocellular carcinoma: results and perspectives. *Front Cell Dev Biol*. 2021;9:674919. doi:10.3389/fcell.2021.674919
22. Tatiparti K, Sau S, Kashaw SK, et al. siRNA delivery strategies: a comprehensive review of recent developments. *Nanomaterials*. 2017;7:77.
23. Singh S. Nanomaterials as non-viral siRNA delivery agents for cancer therapy. *BioImpacts*. 2013;3(2):53–65. doi:10.5681/bi.2013.007
24. Ebrahimi N, Manavi MS, Nazari A, et al. Nano-scale delivery systems for siRNA delivery in cancer therapy: new era of gene therapy empowered by nanotechnology. *Environ Res*. 2023;239(2):117263. doi:10.1016/j.envres.2023.117263
25. Isazadeh H, Oruji F, Shabani S, et al. Advances in siRNA delivery approaches in cancer therapy: challenges and opportunities. *Mol Biol Rep*. 2023;50:9529–9543. doi:10.1007/s11033-023-08749-y
26. Dowdy S, Setten R, Cui X, et al. Delivery of RNA therapeutics: the great endosomal escape! *Nucleic Acid Ther*. 2022;32(5):361–368. doi:10.1089/nat.2022.0004
27. Emami Nejad A, Najafgholian S, Rostami A, et al. The role of hypoxia in the tumor microenvironment and development of cancer stem cell: a novel approach to developing treatment. *Cancer Cell Int*. 2021;21:62. doi:10.1186/s12935-020-01719-5
28. Nie Y, Li D, Peng Y, et al. Metal organic framework coated MnO2 nanosheets delivering doxorubicin and self-activated DNAzyme for chemo-gene combinatorial treatment of cancer. *Int J Pharmaceut*. 2020;585:119513. doi:10.1016/j.ijpharm.2020.119513
29. Wang ZB, Zhang X, Fang C, et al. Immunotherapy and the ovarian cancer microenvironment: exploring potential strategies for enhanced treatment efficacy. *Immunology*. 2024;173(1):14–32. doi:10.1111/imm.13793
30. Wang X, Sun K, Dong J, et al. Carrier-free nanoparticles based on natural products trigger dual “synergy and attenuation” for enhanced phototherapy of liver cancer. *Mater Today Bio*. 2025;35:102278. doi:10.1016/j.mtbio.2025.102278
31. Shi F, Chen L, Wang Y, et al. Enhancement of oral bioavailability and anti-hyperuricemic activity of aloe emodin via novel Soluplus®—glycyrrhizic acid mixed micelle system. *Drug Deliv Transl Res*. 2022;12(3):603–614. doi:10.1007/s13346-021-00969-8
32. Yang Y, Lin, S, Chen, H, et al. Preparation and characterization of linolenic acid-chitosan micelle for doxorubicin oral delivery and its in situ intestinal absorption in rats. *APSB*. 2022;57(9):2857–2863.
33. Wei C, Wang Q, Weng W, et al. The characterisation, pharmacokinetic and tissue distribution studies of TPGS modified myricetrin mixed nanoparticle in rats. *J Microencapsul*. 2019;36(3):278–290. doi:10.1080/02652048.2019.1622606
34. Liu J, Zhu Z, Yang Y, et al. Preparation, characterization, pharmacokinetics, and antirenal injury activity studies of Licochalcone A-loaded liposomes. *J Food Biochem*. 2022;46(1):e14007. doi:10.1111/jfbc.14007
35. Biller LH, Schrag D. Diagnosis and treatment of metastatic colorectal cancer: a review. *JAMA*. 2021;325(7):669–685. doi:10.1001/jama.2021.0106
36. Ma SC, Zhang JQ, Yan TH, et al. Novel strategies to reverse chemoresistance in colorectal cancer. *Cancer Med*. 2023;12(10):1–24.
37. Yoshimura H, Dhar DK, Kohno H, et al. Prognostic impact of hypoxia-inducible factors 1alpha and 2alpha in colorectal cancer patients: correlation with tumor angiogenesis and cyclooxygenase-2 expression. *Clin Cancer Res*. 2004;10:8554–8560. doi:10.1158/1078-0432.CCR-0946-03
38. Kang L, Fan B, Sun P, et al. An effective tumor-targeting strategy utilizing hypoxia-sensitive siRNA delivery system for improved anti-tumor outcome. *Acta Biomater*. 2016;44:341–354. doi:10.1016/j.actbio.2016.08.029
39. He W, Chan CM, Wong SC, et al. Jagged 2 silencing inhibits motility and invasiveness of colorectal cancer cell lines. *Oncol Lett*. 2016;12:5193–5198. doi:10.3892/ol.2016.5321
40. Song H, Wang G, He B, et al. Cationic lipid-coated PEI/DNA polyplexes with improved efficiency and reduced cytotoxicity for gene delivery into mesenchymal stem cells. *Int J Nanomed*. 2012;7:4637–4648. doi:10.2147/IJN.S33923
41. Wang H, He J, Cao D, et al. Synthesis of an acidlabile polymeric prodrug DOX-acetal-PEG-acetal-DOX with high drug loading content for pH-triggered intracellular drug release. *Polym Chem*. 2015;6:4809–4818. doi:10.1039/C5PY00569H
42. Jiang Y, Lu H, Khine YY, et al. Polyion complex micelle based on albumin-polymer conjugates: multifunctional oligonucleotide transfection vectors for anticancer chemotherapeutics. *Biomacromolecules*. 2014;15:4195–4205. doi:10.1021/bm501205x
43. Lukyanov AN, Torchilin VP. nanoparticle from lipid derivatives of water-soluble polymers as delivery systems for poorly soluble drugs. *Adv Drug Deliv Rev*. 2004;56(9):1273–1289. doi:10.1016/j.addr.2003.12.004
44. Sharma A, Arambula JF, Koo S, et al. Hypoxia-targeted drug delivery. *Chem Soc Rev*. 2019;48:771–813. doi:10.1039/c8cs00304a
45. Phung CD, Tran TH, Pham LM, et al. Current developments in nanotechnology for improved cancer treatment, focusing on tumor hypoxia. *J Control Release*. 2020;324:413–429. doi:10.1016/j.jconrel.2020.05.029
46. DE-Souza ASC, Costa-Casagrande TA. Animal models for colorectal cancer. *Arq Bras Cir Dig*. 2018;31(2):e1369. doi:10.1590/0102-672020180001e1369

47. Rajput A, Dominguez San Martin I, Rose R, et al. Characterization of HCT116 human colon cancer cells in an orthotopic model. *J Surg Res*. 2008;147:276–281. doi:10.1016/j.jss.2007.04.021
48. Harrison W, Vicki C, Erian D. 2012. Colon and rectal cancers surprisingly similar. NIH Research Matters. url: https://www.nih.gov/news-events/nih-research-matters/colon-rectal-cancers-surprisingly-similar. Date of searching 2023/5/29. Publisher: Office of Communications and Public Liaison in the NIH Office of the Director.
49. Jensen MM, Jørgensen JT, Binderup T, et al. Tumor volume in subcutaneous mouse xenografts measured by microCT is more accurate and reproducible than determined by 18F-FDG-microPET or external caliper. *BMC Med Imaging*. 2008;8:16. doi:10.1186/1471-2342-8-16
50. Winkels RM, Snetselaar T, Adriaans A, et al. Changes in body weight in patients with colorectal cancer treated with surgery and adjuvant chemotherapy: an observational study. *Cancer Treat Res Commun*. 2016;9:111–115.
51. Tao L, Yang JK, Gu Y, et al. Weichang'an and 5-fluorouracil suppresses colorectal cancer in a mouse model. *World J Gastroenterol*. 2015;21(4):1125–1139. doi:10.3748/wjg.v21.i4.1125
52. VanderVeen BN, Sougiannis AT, Velazquez KT, et al. The acute effects of 5 fluorouracil on skeletal muscle resident and infiltrating immune cells in mice. *Front Physiol*. 2020;11:1–15. doi:10.3389/fphys.2020.593468
53. Sakai H, Kai Y, Takase K, et al. Role of peptide YY in 5-fluorouracil-induced reduction of dietary intake. *Clin Exp Pharmacol Physiol*. 2016;43(8):753–759. doi:10.1111/1440-1681.12588
54. Meyerhardt JA, Niedzwiecki D, Hollis D, et al. Impact of body mass index and weight change after treatment on cancer recurrence and survival in patients with stage III colon cancer: findings from Cancer and Leukemia Group B 89803. *J Clin Oncol*. 2008;26(25):4109–4115. doi:10.1200/JCO.2007.15.6687
55. Atalay C, Küçük Aİ. The impact of weight gain during adjuvant chemotherapy on survival in breast cancer. *Ulus Cerrahi Derg*. 2015;31(3):124–127. doi:10.5152/UCD.2015.3123
56. Chen Z, Han F, Du Y, et al. Hypoxic microenvironment in cancer: molecular mechanisms and therapeutic interventions. *Signal Transduction Tar*. 2023;8:70.
57. Bigos KJA, Quiles CG, Lunj S, et al. Tumour response to hypoxia: understanding the hypoxic tumour microenvironment to improve treatment outcome in solid tumours. *Front Oncol*. 2024;14:1331355. doi:10.3389/fonc.2024.1331355
58. Dewhirst M, Secomb T. Transport of drugs from blood vessels to tumour tissue. *Nat Rev Cancer*. 2017;17:738–750. doi:10.1038/nrc.2017.93
59. Yang R, Chen L, Wang Y, et al. Tumor microenvironment responsive metal nanoparticles in cancer immunotherapy. *Front Immunol*. 2023;14:1237361. doi:10.3389/fimmu.2023.1237361